Universiteit Leiden
The Netherlands

The metallophilic interaction between cyclometalated complexes: photobiological applications

Zhou, X.

Citation
Zhou, X. (2021, May 26). *The metallophilic interaction between cyclometalated complexes: photobiological applications*. Retrieved from https://hdl.handle.net/1887/3158746

Version:	Publisher's Version
License:	Licence agreement concerning inclusion of doctoral thesis in the Institutional Repository of the University of Leiden
Downloaded from:	https://hdl.handle.net/1887/3158746

Note: To cite this publication please use the final published version (if applicable).

Cover Page

Universiteit Leiden

Leiden University Repository

The handle #https://hdl.handle.net/1887/3158746 holds various files of this Leiden University dissertation.

Author: Zhou, X.
Title: The metallophilic interaction between cyclometalated complexes: photobiological applications
Issue Date: 2021-04-08

APPENDIX I SUPPORTING INFORMATION FOR CHAPTER 2

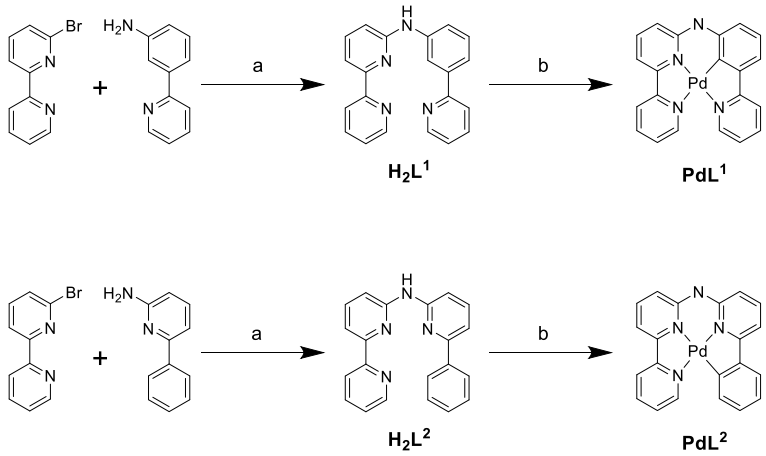

Scheme AI.1 (a) Toluene, BINAP, $Pd(dba)_2$, KO*t*-Bu, 85 °C, N_2, 3 days; (b) CH_3COOH, N_2, 135 °C, 12 h.

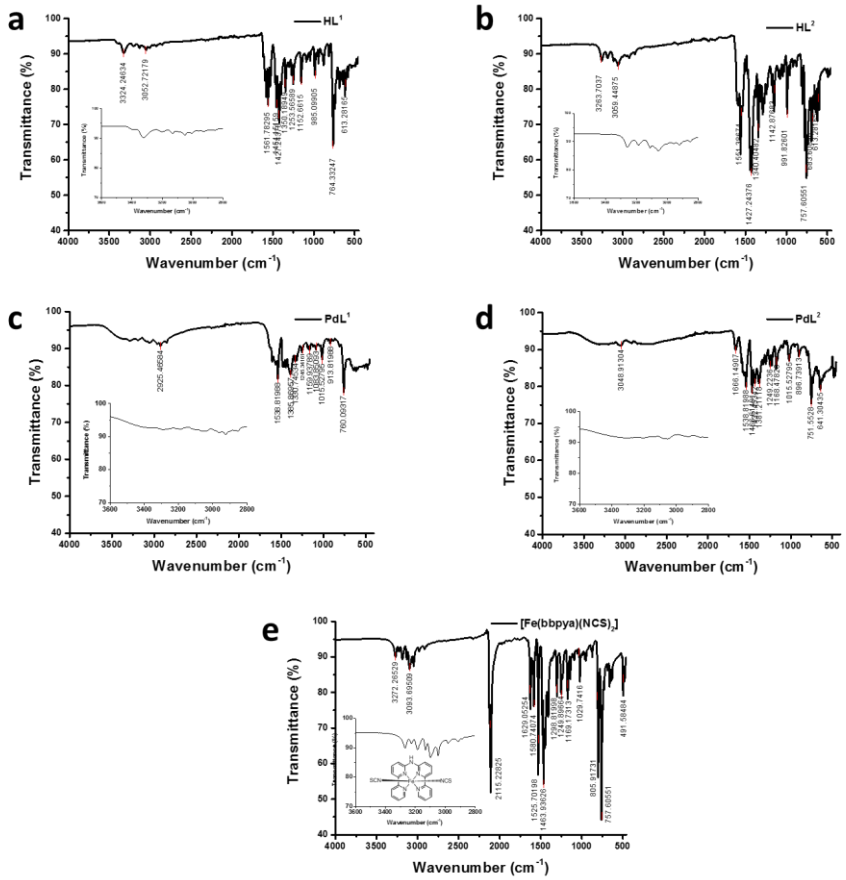

Figure AI.1 IR spectra of ligands **HL^1** (a), **HL^2** (b), palladium complexes **PdL^1** (c), **PdL^2** (d), and the reference complex $[Fe(bbpya)(NCS)_2]$ (e).

Table AI.1 Crystallographic Data for **PdL²**

Complex	**PdL²**
Crystal data	
Chemical formula	$C_{21}H_{14}N_4Pd$
M_r	428.76
Crystal system, space group	Monoclinic, $P2_1/n$
Temperature (K)	110
a, b, c (Å)	10.3734 (3), 7.2412 (2), 20.6547 (6)
β (°)	100.020 (3)
V (Å^3)	1527.83 (8)
Z	4
Radiation type	Mo $K\alpha$
μ (mm^{-1})	1.23
Crystal size (mm)	0.23 × 0.11 × 0.04
Data collection	
Diffractometer	SuperNova, Dual, Cu at zero, Atlas
Absorption correction	Gaussian *CrysAlis PRO* 1.171.39.29c (Rigaku Oxford Diffraction, 2017) Numerical absorption correction based on gaussian integration over a multifaceted crystal model Empirical absorption correction using spherical harmonics, implemented in SCALE3 ABSPACK scaling algorithm.
T_{min}, T_{max}	0.625, 1.000
No. of measured, independent and observed [$I > 2\sigma(I)$] reflections	20278, 3517, 3063
R_{int}	0.036
$(\sin \theta/\lambda)_{max}$ (Å^{-1})	0.650
Refinement	
$R[F^2 > 2\sigma(F^2)]$, $wR(F^2)$, S	0.025, 0.060, 1.07
No. of reflections	3517
No. of parameters	320
No. of restraints	581
H-atom treatment	H-atom parameters constrained
$\Delta\rho_{max}$, $\Delta\rho_{min}$ (e Å^{-3})	0.88, -0.79

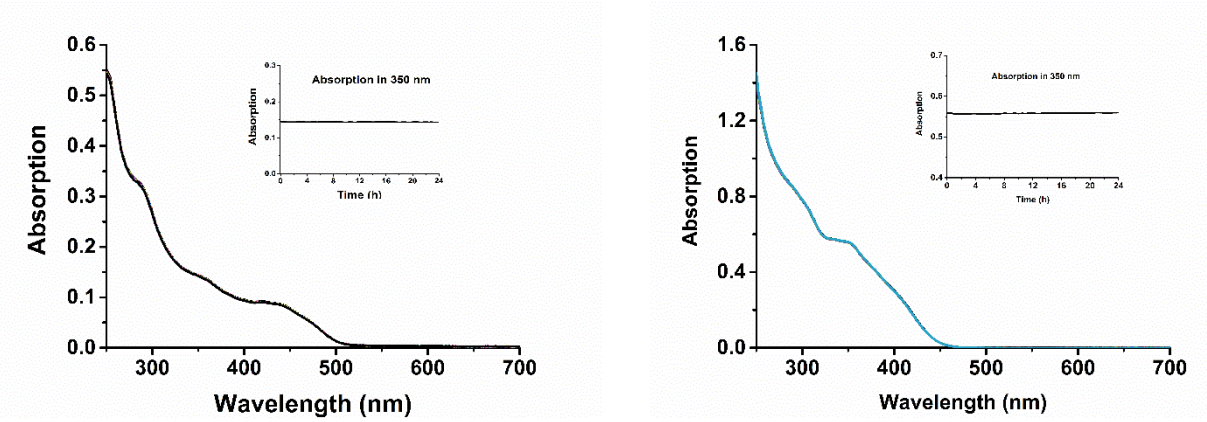

Figure AI.2 Time-evolution of the absorption spectra of **PdL¹** (left) and **PdL²** (right) in PBS: DMSO (50 µm, 1:1) solution at 310 K for 24 hours. The spectra were measured every 30 min.

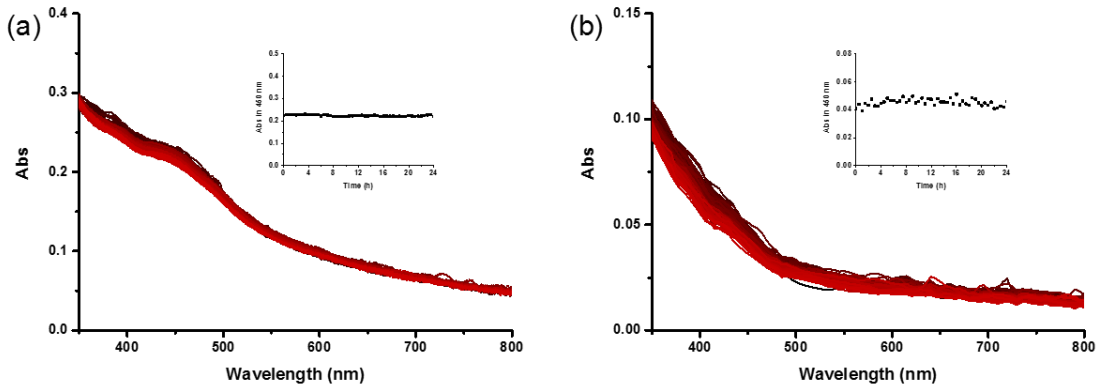

Figure AI.3 Evolution of the absorption spectrum of complexes **PdL¹** (a) and **PdL²** (b) when incubated in Opti-MEM containing 2.5% FCS at 310 K for 24 hours. The spectra were measured every 30 min. Inset: time evolution of the absorbance at 450 nm. The color of spectra change from black (0 h) to red (24 h).

Table AI.2 Octanol-water partition coefficients (log P_{ow}) of the two palladium complexes.

Complex	log P_{ow}
PdL¹	-0.64
PdL²	0.046

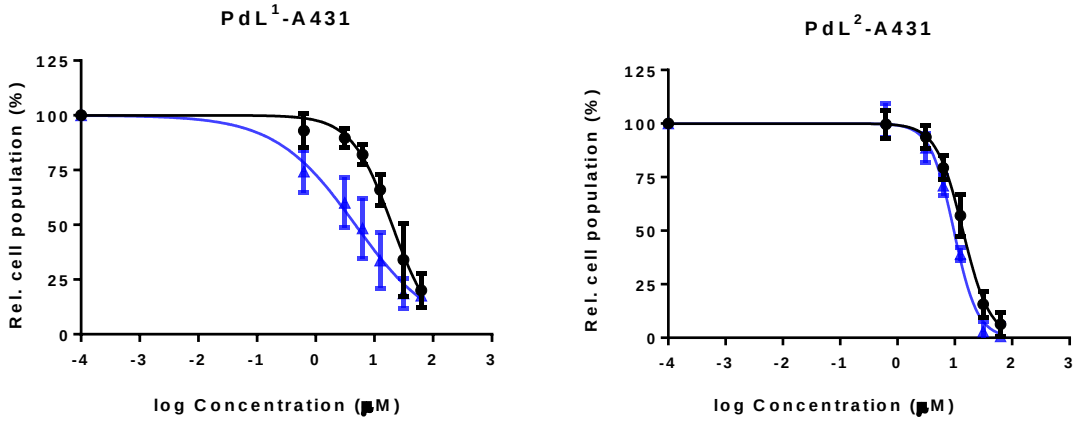

Figure AI.4 Dose-response curves for A431 cells incubated with palladium complexes and irradiated 5 min with blue light (blue data points), or left in the dark (black data points). Photocytoxicity assay outline: cells seeded at 5 × 10^3 cells/well at t = 0 h; treated with **PdL¹** or **PdL²** at t = 24 h; irradiated at t = 48 h, blue light (455 nm, 5 min, 10.5 mW cm^{-2}, 3.2 J cm^{-2}); SRB assay performed at t = 96 h. Incubation conditions: 37 °C, 21% O_2, 7% CO_2.

Table AI.3 Photophysical data for **PdL¹** and **PdL²**

Complex	λ_{abs}, nm (ε x 10^3 M^{-1} cm^{-1})[a]	λ_{em} (nm)[b]	φ_P [b]	φ_Δ [b]	Lifetime (ns)[a,c]	
					τ_1	τ_2
PdL¹	251 (26.8), 286 (17.1), 422 (4.3)	539	0.0017	0.89	0.271±0.002 (97%)	6.4±0.3 (3%)
PdL²	283 (16.7), 347 (11.7)	604	0.00084	0.38	0.333±0.005 (96%)	5.3±0.5 (4%)

[a] Measurements were carried out in methanol. [b] Measurements were carried out at 450 nm excitation wavelength and in a solution of deuterated methanol in air atmosphere according to literature. The absorption of complexes at 450 nm were set below 0.1 to avoid the generation of excimer. A solution of $[Ru(bpy)_3]Cl_2$ (Tris(2,2'-bipyridyl)dichlororuthenium(II)) in deuterated methanol (photoluminescence quantum yield φ_P = 0.015, singlet oxygen quantum yield φ_Δ = 0.73) was used as reference. [c] Excitation source 375 nm. Biexponential model: $y = y_0 + A_1*\exp(-(x-x_0)/\tau_1) + A_2*\exp(-(x-x_0)/\tau_2)$

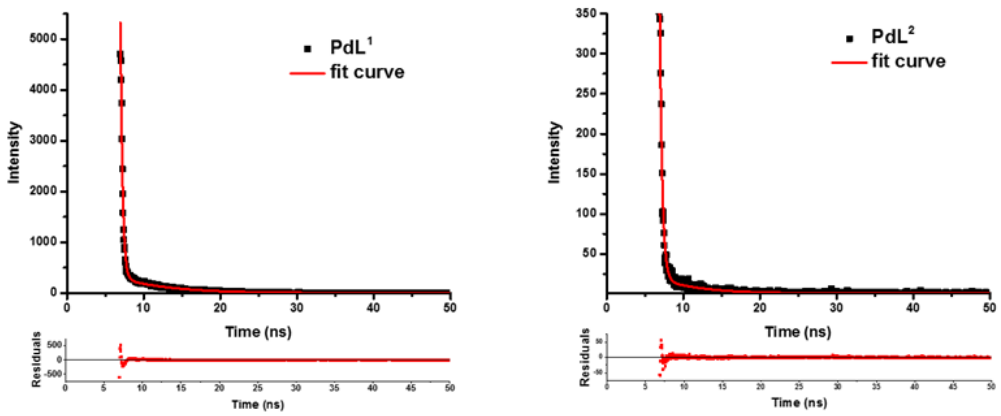

Figure AI.5 The phosphorescence lifetime spectra and fit curve of palladium complexes in methanol. Fit equation: $y = y_0 + A_1*\exp(-(x-x_0)/\tau_1) + A_2*\exp(-(x-x_0)/\tau_2)$.

Table AI.4 HOMO and LUMO energies, Energy gap (ΔE) of **PdL¹** and **PdL²**

Complex	LUMO/eV	HOMO/eV	ΔE/eV
PdL¹	-2.048	-5.258	3.21
PdL²	-2.114	-5.644	3.53

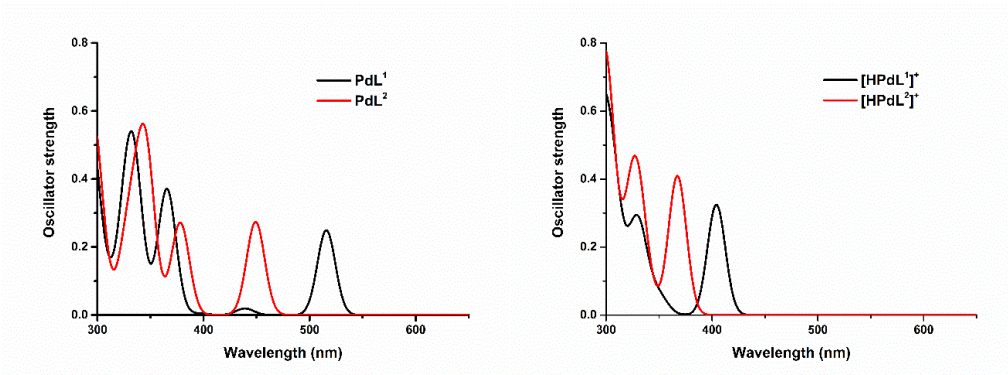

Figure AI.6 TDDFT-calculated spectra for **PdL¹**, **PdL²** (left) and **[PdHL¹]⁺, [PdHL²]⁺** (right) at the TZP/COSMO level in methanol. The theoretical curves were calculated and plotted in ADF with Gaussian Fixed Oscillator Strengths. Scaling factor = 1.0, peak width = 30 nm.

APPENDIX II SUPPORTING INFORMATION FOR CHAPTER 3

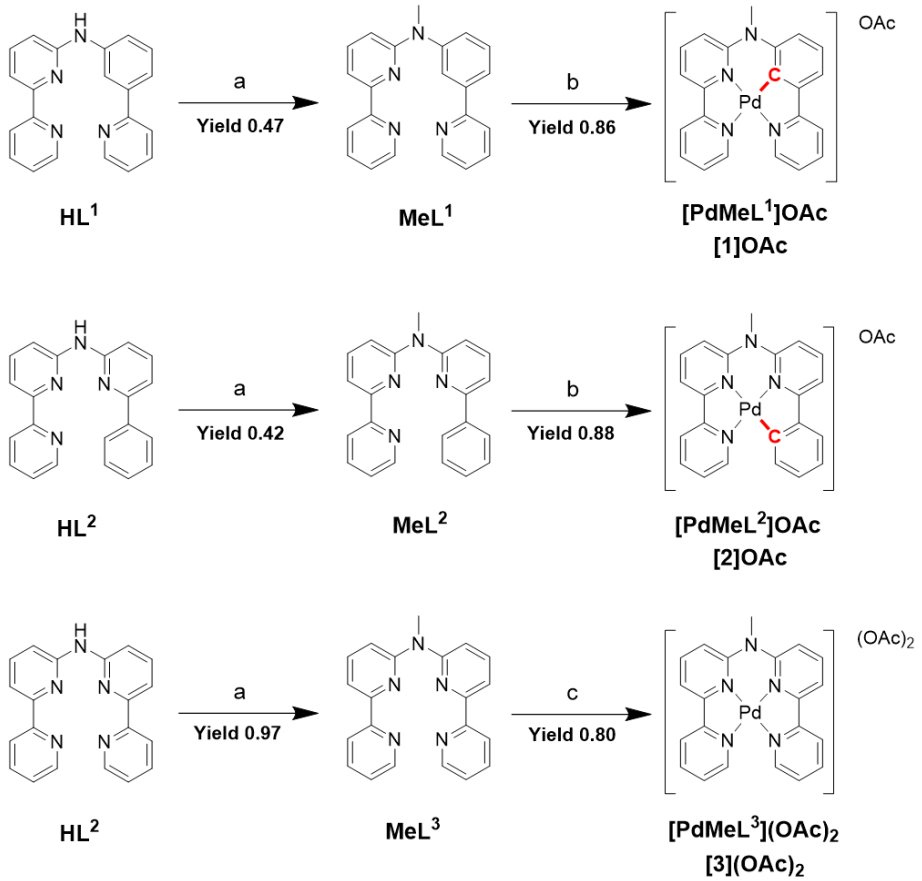

Scheme AII.1 Synthesis of ligands **MeL^1-MeL^3** and of their palladium complexes. Reaction condition: (a) CH_3I, KO*t*-Bu, DMF, room temperature, 24 h; (b) palladium(II) acetate, CH_3COOH, N_2, 135 °C, 24 h; (c) Palladium(II) acetate, MeOH, 65 °C, 24 h.

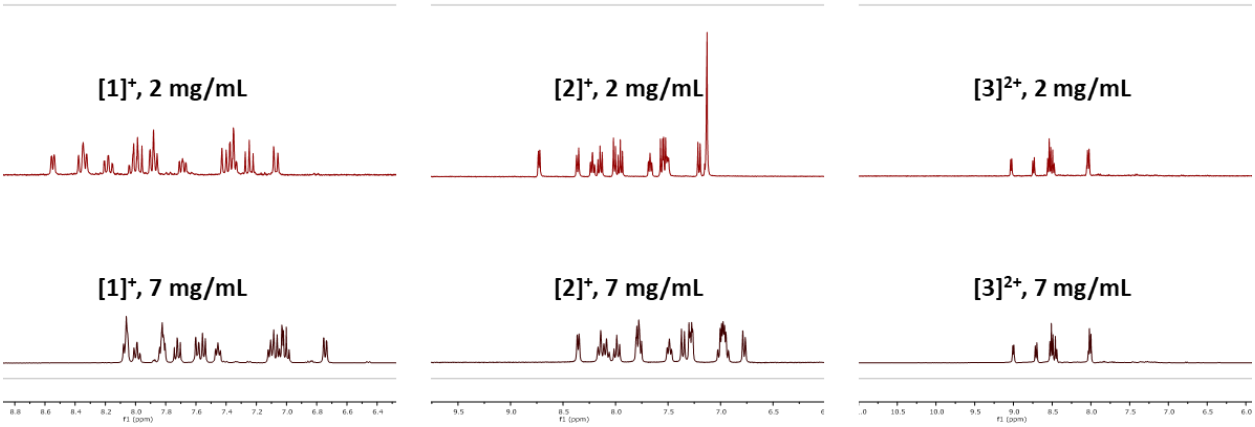

Figure AII.1 The aromatic region of the ^{1}H NMR spectrum of complexes **[1]$^+$-[3]$^{2+}$** at low (2 mg/mL) and high (7 mg/mL) concentration. Solvent: CD_3OD.

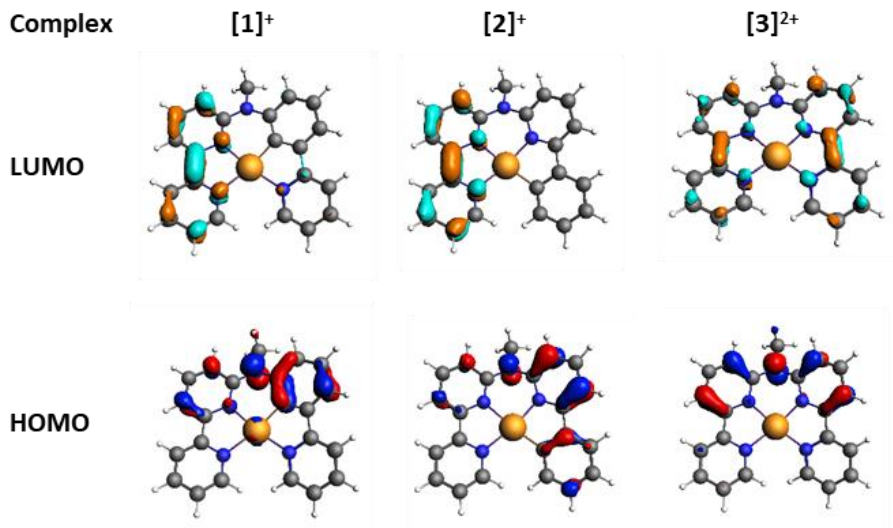

Figure AII.2 DFT calculation of HOMOs (bottom) and LUMOs (top) orbitals of **[1]**$^{+}$**-[3]**$^{2+}$; occupied orbitals (HOMO) have red and blue lobes, and unoccupied orbitals (LUMO) brown and cyan lobes. Element color code: grey = C; orange = Pd; blue = N; white = H. Level of theory: ADF/DFT/PBE0/TZP/COSMO(water).

Table AII.2 HOMO and LUMO energies, energy gap (ΔE) of complexes **[1]**$^{+}$**-[3]**$^{2+}$.

Complex	HOMO /eV	LUMO/eV	ΔE/eV
[1]$^{+}$	-6.24	-2.41	3.83
[2]$^{+}$	-6.58	-2.46	4.11
[3]$^{2+}$	-6.95	-2.82	4.13

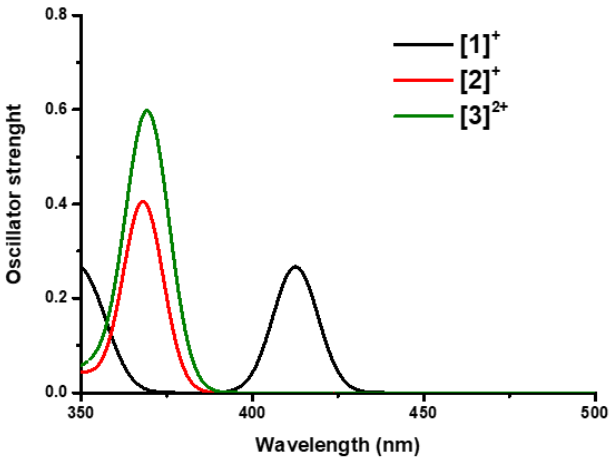

Figure AII.3 TDDFT-calculated spectra for palladium complexes **[1]**$^{+}$**-[3]**$^{2+}$. Level of theory: ADF/TDDFT/PBE0/TZP/COSMO (water).

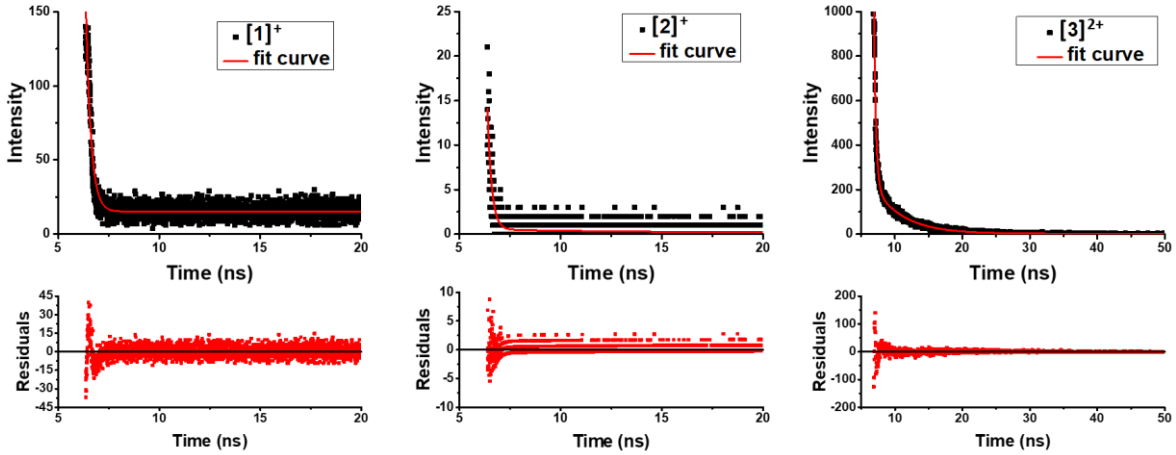

Figure AII.4 The phosphorescence lifetime spectra and fit curve of complexes **[1]$^{+}$-[3]$^{2+}$** in water under air atmosphere at room temperature. Fit equation: $y = y_0 + A_1*\exp(-(x-x_0)/\tau_1)$ (**[1]$^{+}$** and **[2]$^{+}$**, $y = y_0 + A_1*\exp(-(x-x_0)/\tau_1) + A_2*\exp(-(x-x0)/\tau_2)$ (**[3]$^{2+}$**). Excitation wavelength: 375 nm. The data were analysized via OriginPro 9.1.

Table AII.5 The derived countrate (kcps) values of complexes in different solutions and different concentrations.

complex		H_2O	PBS	Opti-MEM with FCS	Opti-MEM without FCS	Opti-MEM with BSA
Solution only		54	40	894	107	8257
[1]$^{+}$	5 µM	37	65	2268	1936	
	50 µM	146	187	19144	18970	14105
[2]$^{+}$	5 µM	30	58	2775	5657	
	50 µM	67	61	22311	25377	13359
[3]$^{2+}$	5 µM	56	60	927	136	
	50 µM	79	21	930	101	8056

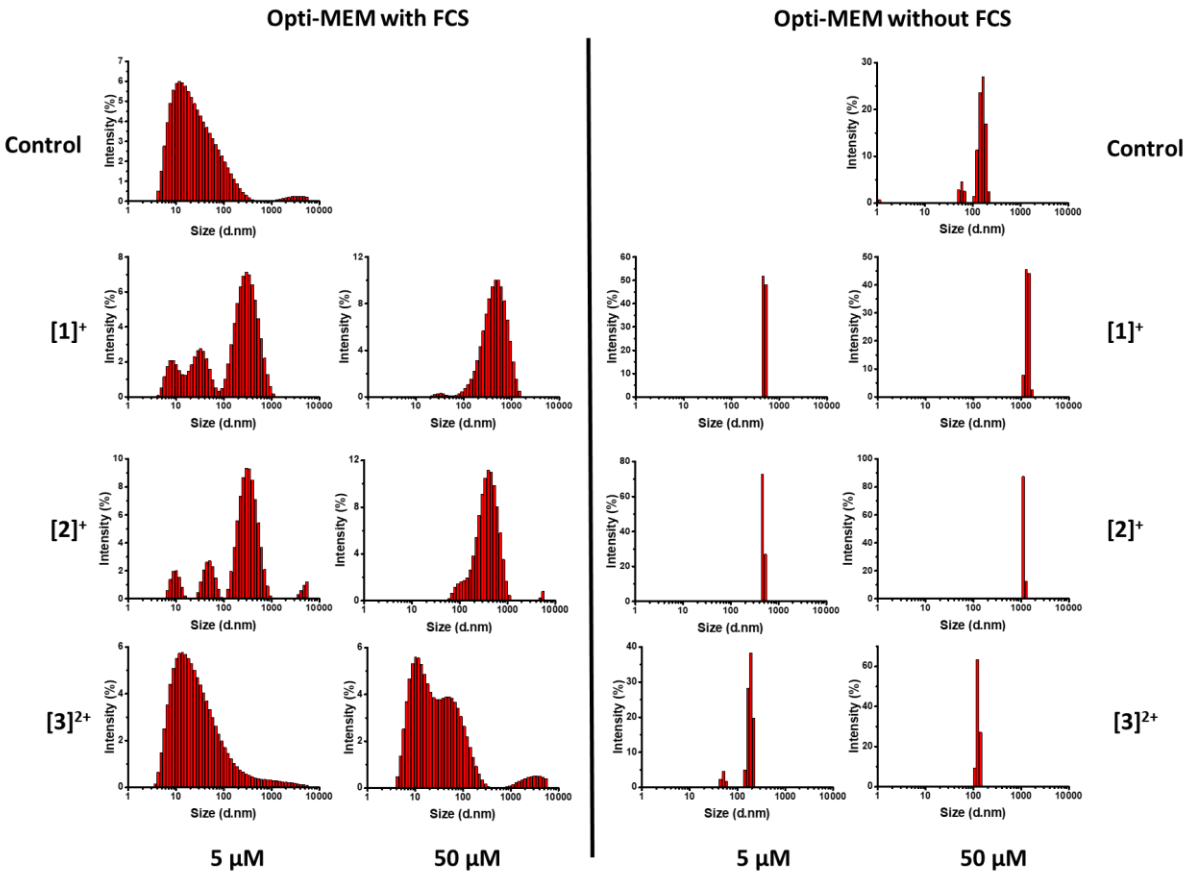

Figure AII.5 Size distributions according to DLS of solution of **[1]OAc-[3]OAc** at 5 or 50 µM in different solvents.

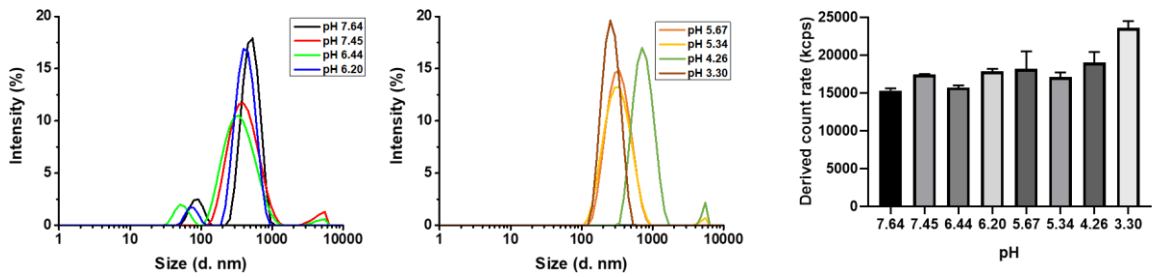

Figure AII.6 DLS size distribution (left and middle) and derived count rate (right) of **[1]OAc** (50 µM) in Opti-MEM complete medium at different pH.

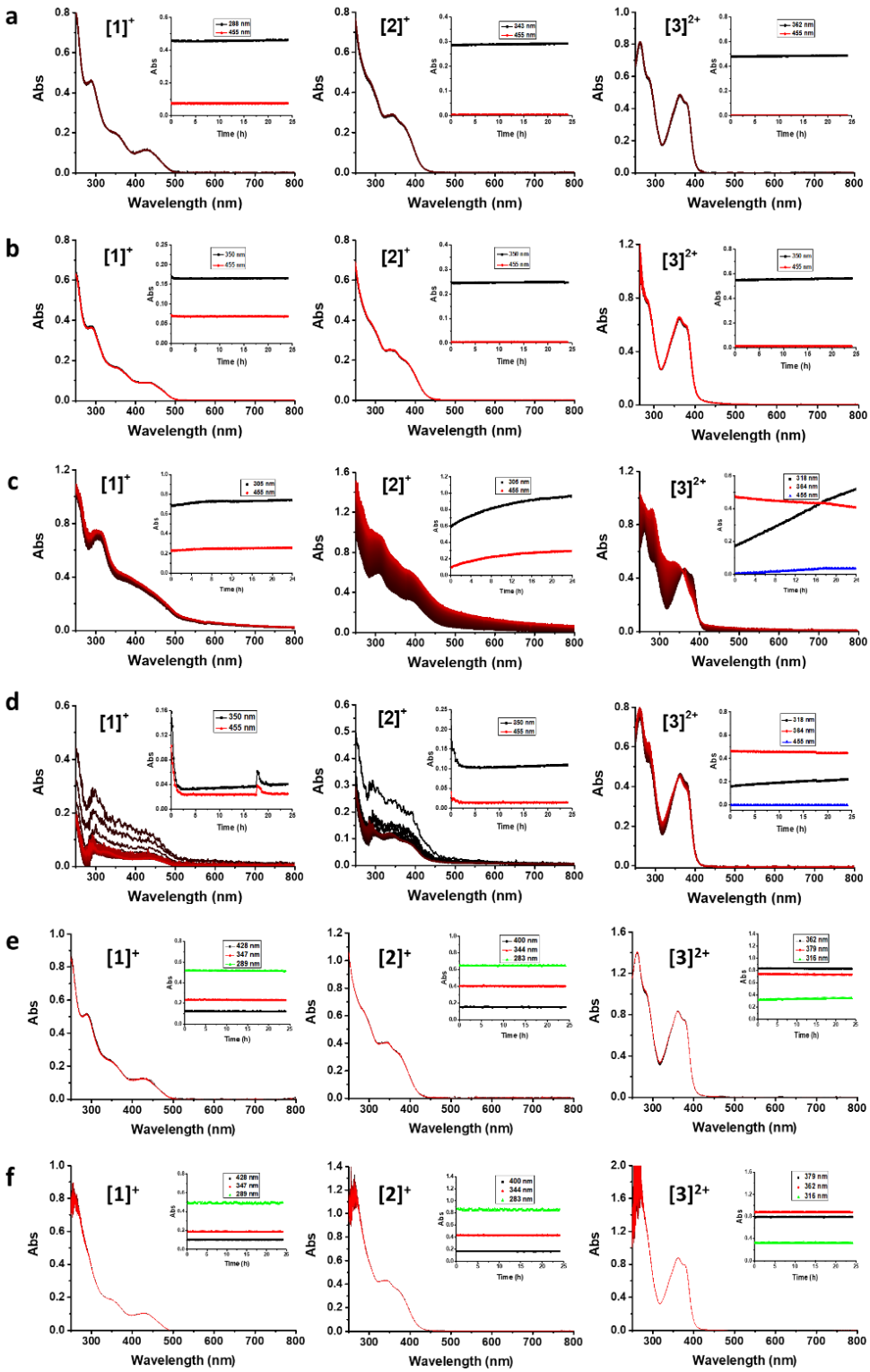

Figure AII.7 Time evolution of the absorbance spectra of solutions of **[1]$^{+}$-[3]$^{2+}$** in H_2O (a), PBS (b), cell medium with FCS (c), cell medium without FCS (d), H_2O with GSH (200 µM, e) and H_2O with ascorbic acid (200 µM, f) at 310 K. Concentration 50 µM. The color change of the spectra indicates the time, with black corresponding to the first curve (0 h) and red to the last one (24 h).

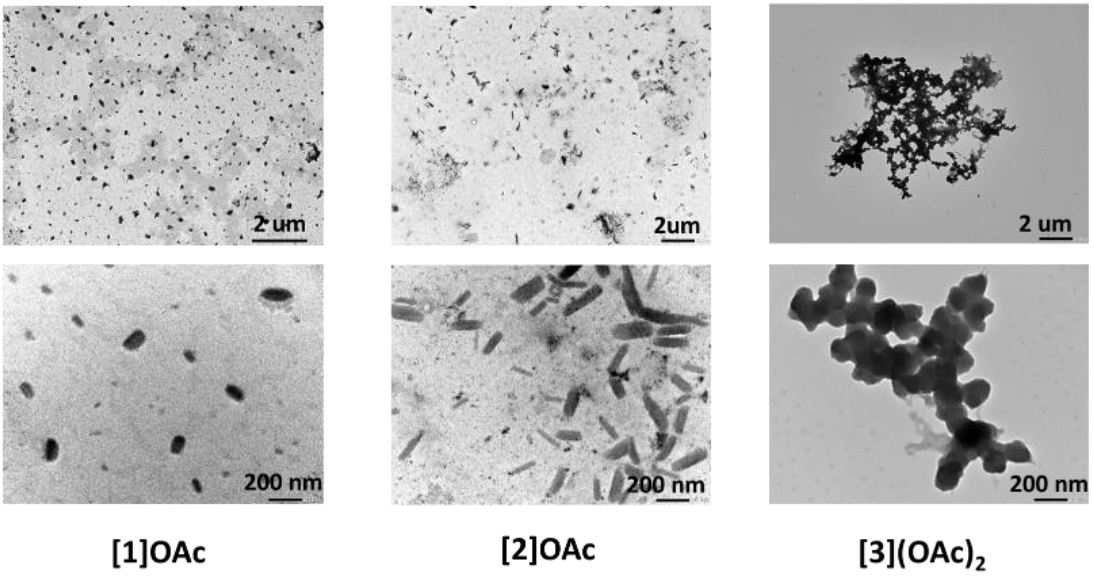

Figure AII.8 TEM images of samples prepared from evaporated MilliQ water solutions of **[1]OAc**, **[2]OAc**, and **[3](OAc)2** (50 µM). Scale bar: 2 µm (top) and 200 nm (bottom).

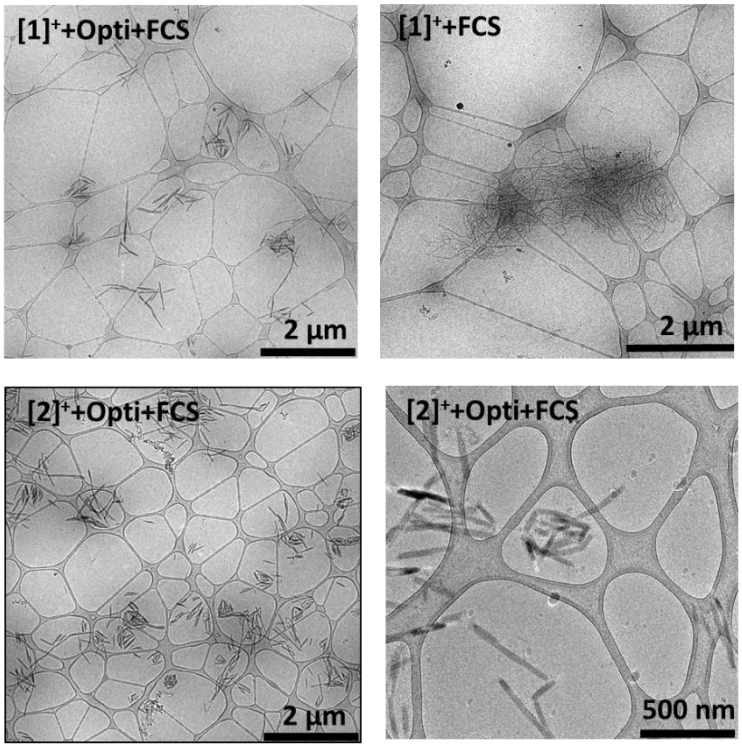

Figure AII.9 The Cryo-TEM images of complexes **[1]**$^+$**-[2]**$^+$ (50 µM) in the Opti-MEM medium with or without FCS.

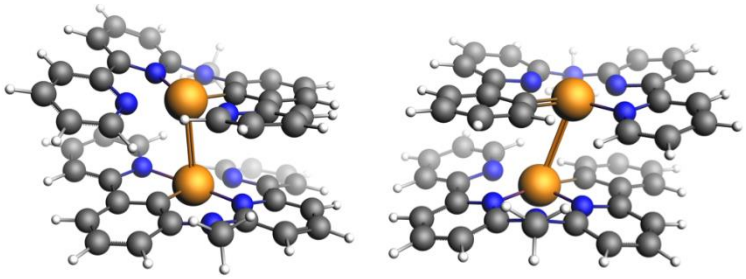

Figure AII.10 Structures of the DFT-optimized dimers $\{[\mathbf{1}]^+\}_2$ (left) and $\{[\mathbf{2}]^+\}_2$ (right).

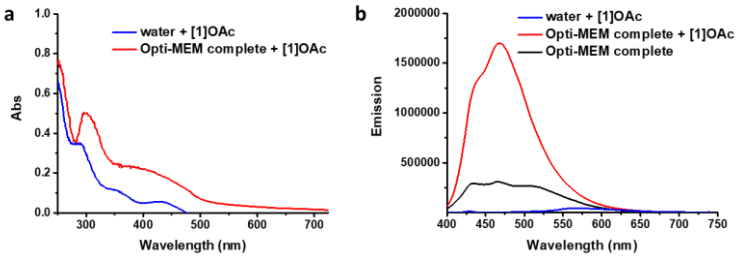

Figure AII.11 The absorbance (a) and emission spectra (b) of **[1]OAc** (50 µM) in water and Opti-MEM complete medium.

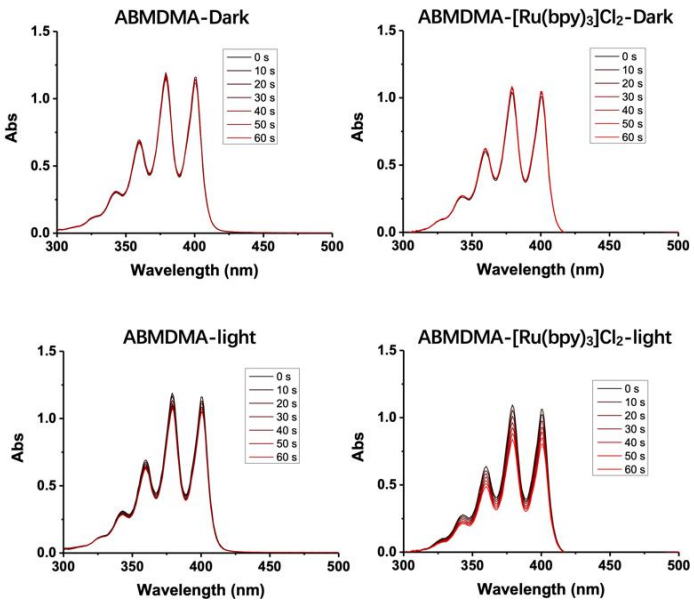

Figure AII.12 The absorbance of ABMDMA Opti-MEM complete solution (100 µM) in the absence or presence of $[Ru(bpy)_3]Cl_2$ (50 µM) under dark or blue light (450 nm) irradiation. (b) Absorbance time evolution and linear fit curve at 378 nm of ABMDMA Opti-MEM complete solution (100 µM) in the absence or presence of **[1]OAc** (50 µM), $[Ru(bpy)_3]Cl_2$ (50 µM) under blue light irradiation. The baseline for these spectra was a solution of **[1]OAc** (50 µM) or $[Ru(bpy)_3]Cl_2$ (50 µM) in Opti-MEM medium without ABMDMA.

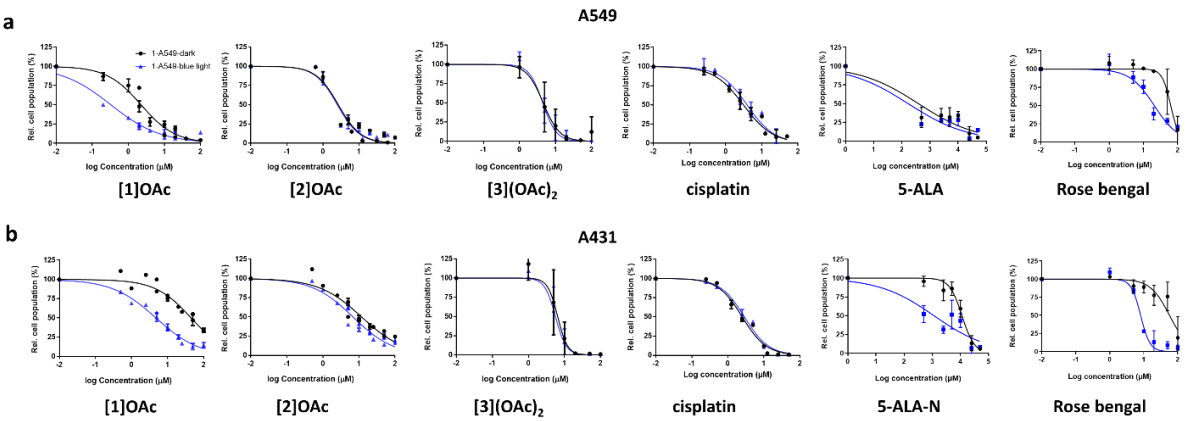

Figure AII.13 Dose-response curves for A549 and A431 cancer cells incubated with complexes **[1]OAc-[3](OAc)2** and cisplatin, either in the dark (black data points) or upon blue light irradiation (5 minutes, 5.66 mW cm^{-2}, 1.7 J cm^{-2}, blue data points), under normoxic condition (37 °C atmosphere, 21% O_2 and 7.0% CO_2).

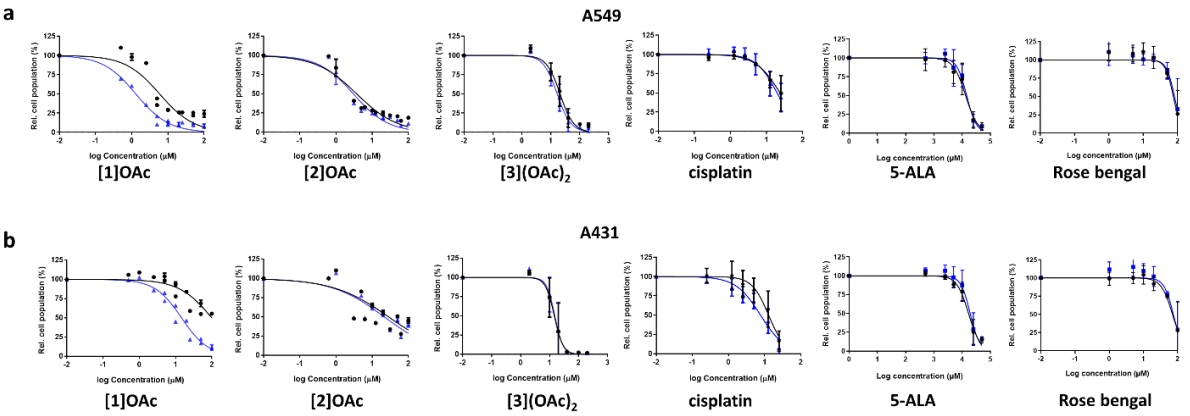

Figure AII.14 Dose-response curves for A549 and A431cancer cells incubated with complexes **[1]OAc-[3](OAc)2**, cisplatin, 5-ALA and Rose bengal either in the dark (black data points) or upon blue light irradiation (455 nm, 8 min, 3.54 mW cm^{-2}, 1.7 J cm^{-2}, blue data points) under hypoxic condition (37 °C atmosphere, 1% O_2 and 7.0% CO_2).

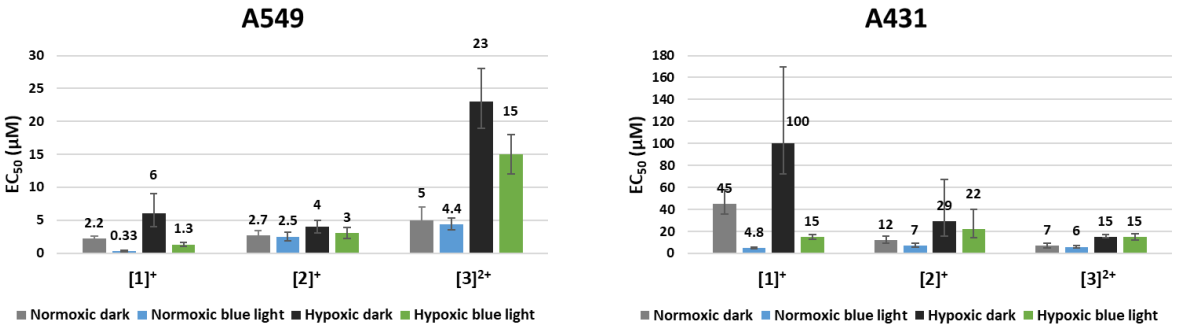

Figure AII.15 Graphical representation of the EC_{50} values of complexes **[1]OAc-[3](OAc)2** in A549 and A431 in the dark or upon blue light irradiation, in normoxic vs. hypoxic conditions. (irradiation condition: normoxic 455 nm, 5 minutes, 5.66 mW cm^{-2}, 1.7 J cm^{-2}, hypoxic 455 nm, 8 min, 3.54 mW cm^{-2}, 1.7 J cm^{-2}).

Table AII.7 Palladium cellular uptake according to ICP-MS analysis in the different fractions of A549 cells treated with **[1]OAc-[3](OAc)$_2$** (1 µM) in the dark after 24 h.

Complex	Treatment (ng Pd)	Metal uptake (ng Pd/million cells)	Metal uptake efficiency (%)	Fractions	Metal distribution (ng Pd/million cells)	Relative metal distribution (%)
[1]OAc	212.84	19±7	5.2	cytosol membranes nucleus cytoskeleton	0.7±0.1 0.23±0.03 0.23±0.03 17±3	3.5 1.1 1.1 94.3
[2]OAc	212.84	14±4	9.8	cytosol membranes nucleus cytoskeleton	0.45±0.05 0.68±0.09 0.34±0.04 12±2	3.3 5.1 2.5 89.1
[3](OAc)$_2$	212.84	1.7±0.2	0.8	cytosol membranes nucleus cytoskeleton	0.42±0.09 0.28±0.06 0 1.1±0.2	23.3 15.6 0 61.1

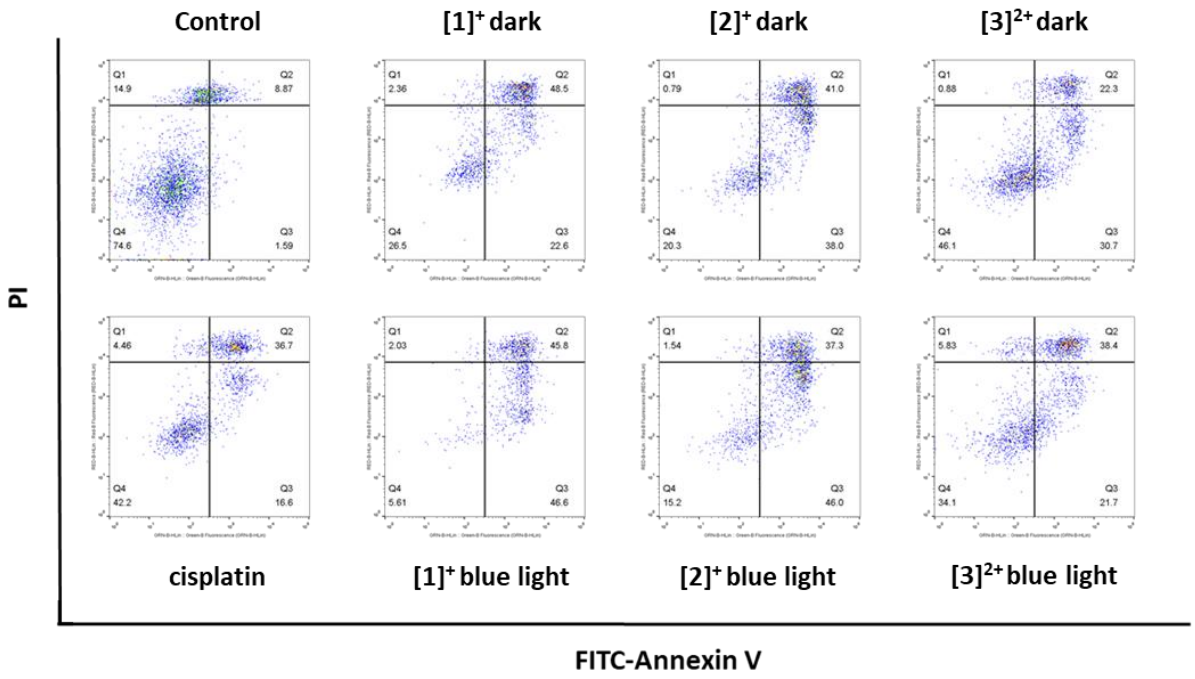

Figure AII.16 Annexin V/propidium iodide double staining FACS data for A549 cells after treatment with cisplatin (15 µM) and complexes **[1]OAc-[3](OAc)$_2$** (15 µM) in the dark or upon blue light irradiation (455 nm, 5 minutes, 5.66 mW cm^{-2}, 1.7 J cm^{-2}).

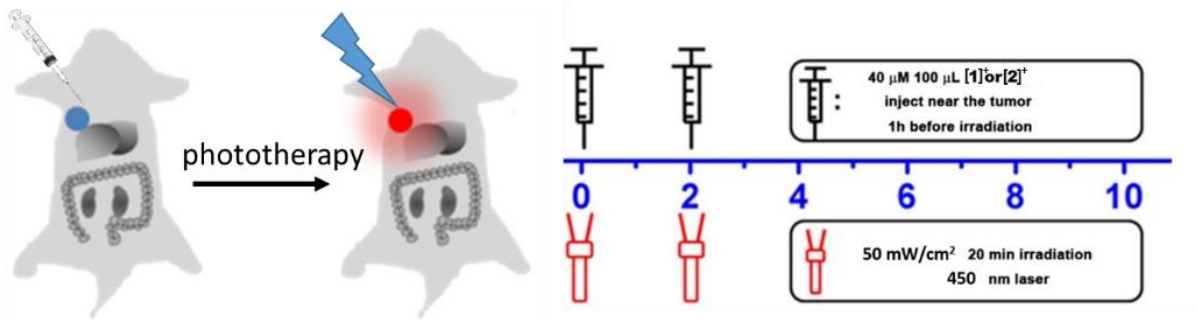

Scheme AII.2 The sketch of *in vivo* experiments for complexes **[1]**$^+$ and **[2]**$^+$.

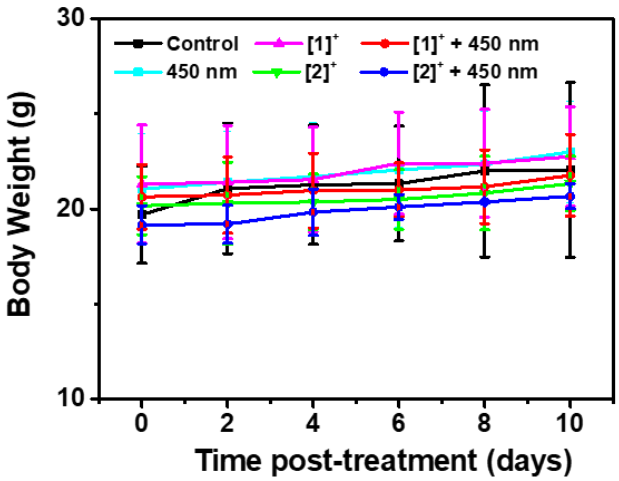

Figure AII.17. Bodyweight of mice treated with **[1]OAc** and **[2]OAc** and control groups.

APPENDIX III SUPPORTING INFORMATION FOR CHAPTER 4

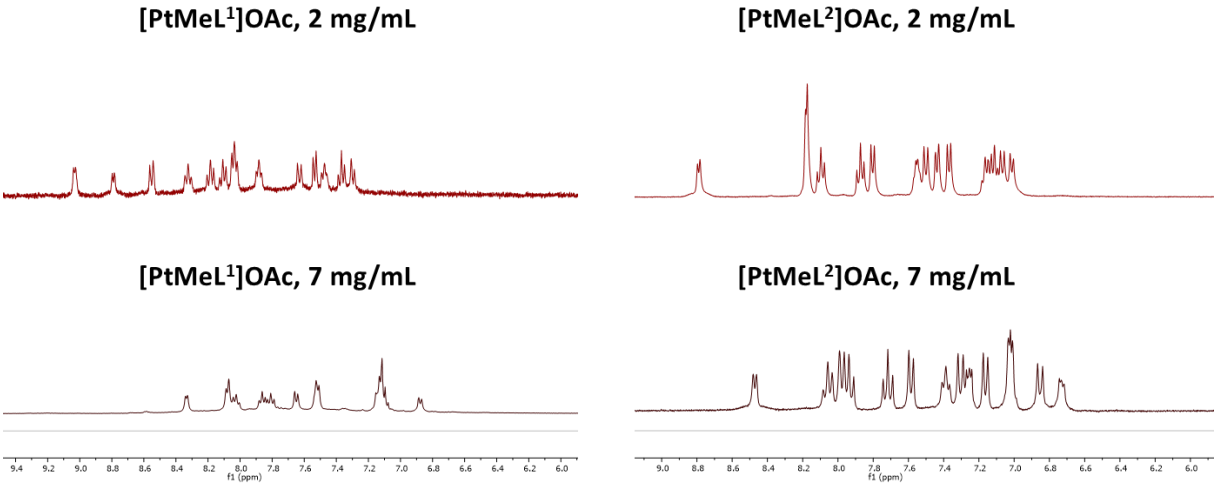

Figure AIII.1 ^{1}H NMR of complexes **[PtMeL^{2}]OAc** and **[PtMeL^{2}]OAc** at low (2 mg/mL MeOD) and high (7 mg/mL MeOD) concentration.

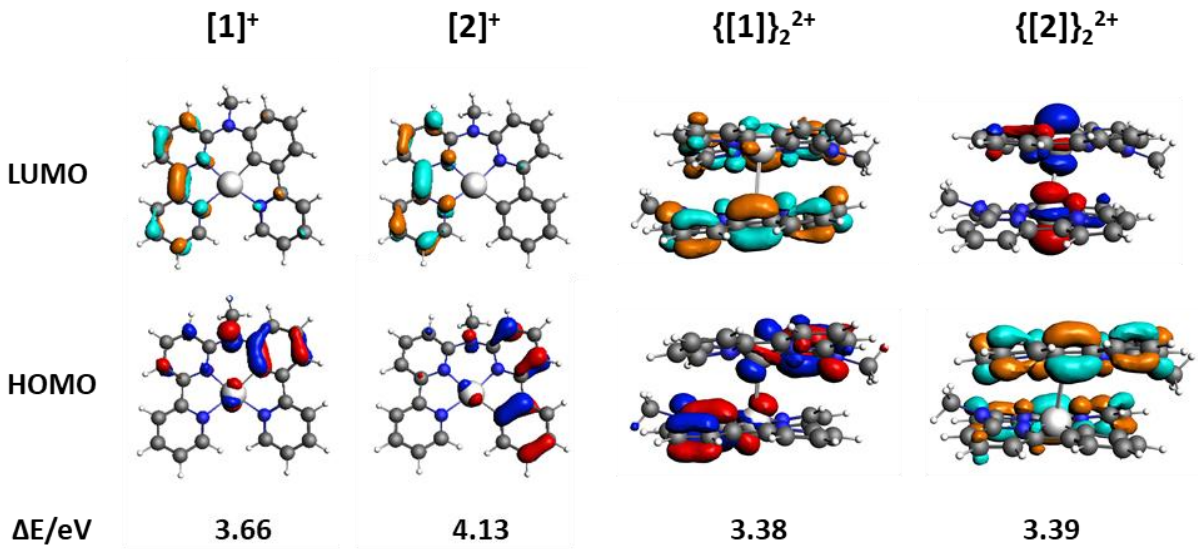

Figure AIII.2 (a) DFT calculation of HOMOs (bottom) and LUMOs (top) orbitals of **[1]**$^{+}$ and **[2]**$^{+}$ in monomer and dimer states. Occupied orbitals (HOMO) have red and blue lobes, and unoccupied orbitals (LUMO) brown and cyan lobes. Element color code: blue = N, grey = C, white = Pt and H.

Table AIII.1 The lowest (λ>350 nm) and most intense (f > 0.01) TDDFT singlet-singlet transitions calculation information of platinum complexes in monomer and dimer states.

Complex	Energy (nm)	Energy (eV)	Oscillator strength (f)	Orbital transition contribution
[1]$^{+}$	370.3522	3.3477	0.3260	65.1% HOMO-1→LUMO 26.0% HOMO→LUMO+1
	441.1625	2.8104	0.2223	96.8% HOMO→LUMO
[2]$^{+}$	375.1118	3.3053	0.4247	61.0%% HOMO-1→LUMO 35.7%% HOMO→LUMO
|[1]$_2$|$^{2+}$	518.4094	2.3916	0.0188	78.3% HOMO→LUMO
	471.8107	2.6278	0.0996	93.8% HOMO→LUMO
	454.6116	2.7273	0.0203	15.3% HOMO-2→LUMO 11.9% HOMO-1→LUMO+1
|[2]$_2$|$^{2+}$	473.1412	2.6204	0.0163	83.3% HOMO→LUMO
	447.1158	2.7730	0.0697	93.5%HOMO→LUMO
	413.8552	2.9958	0.0506	91.8% HOMO-1→LUMO

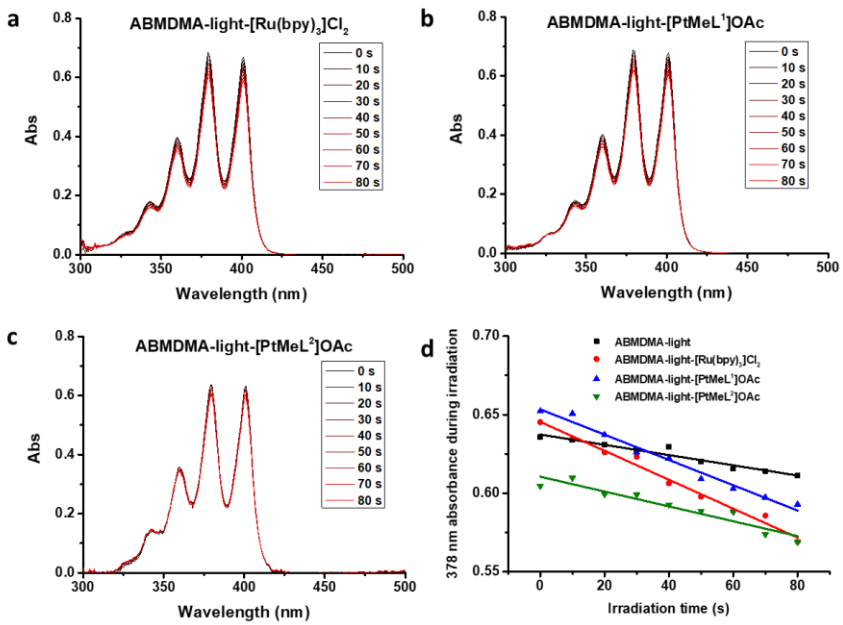

Figure AIII.3 Singlet oxygen generation of aggregates of **[1]OAc-[2]OAc** and reference $[Ru(bpy)_3]Cl_2$ in Opti-MEM complete medium. (a-c) The absorbance change of ABMDMA (100 μM) in Opti-MEM complete in presence of **[1]OAc-[2]OAc** or reference $[Ru(bpy)_3]Cl_2$ (50 μM) upon blue light irradiation (d) Evolution of the absorbance at 378 nm vs. irradiation time of ABMDMA (100 μM) in Opti-MEM complete medium in the absence or presence of **[1]OAc-[2]OAc** or reference $[Ru(bpy)_3]Cl_2$ (50 μM) under blue light irradiation. Irradiation conditions: 298 K, 450 nm, 5.23 mW cm^{-2}, 80 s.

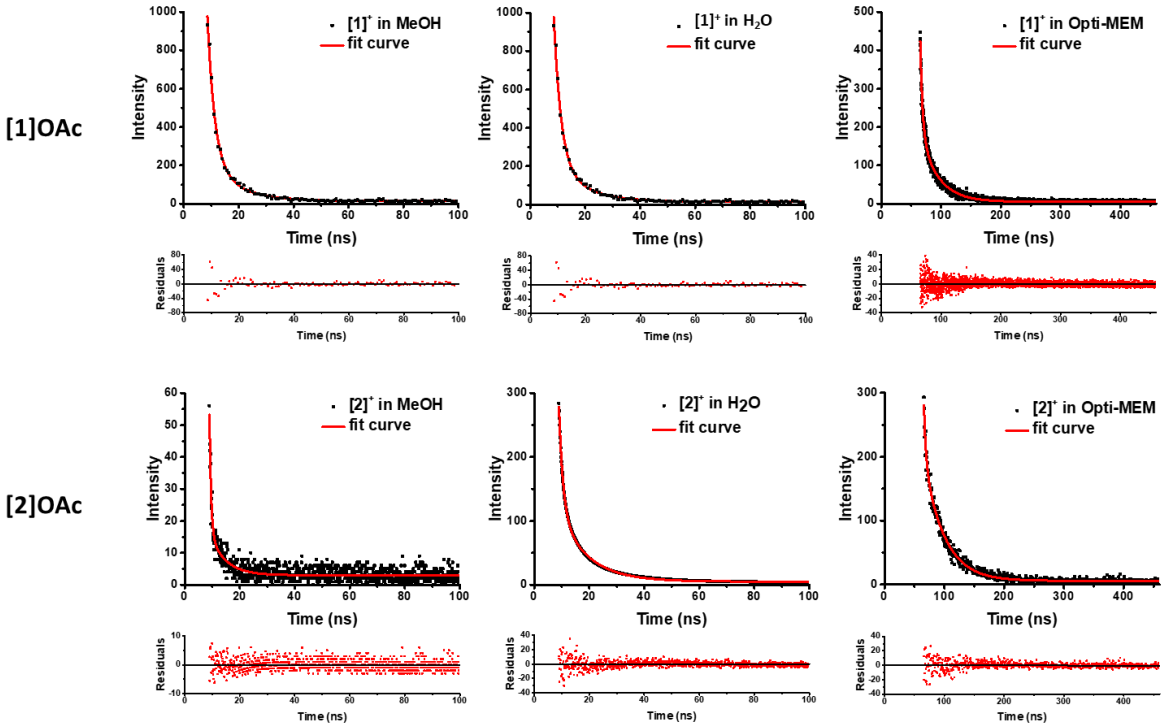

Figure AIII.4 The phosphorescence lifetime spectra and fitting curves for platinum complexes **[1]OAc** and **[2]OAc** in aerated methanol, water and Opti-MEM. Fit equation: $y = y_0 + A_1*\exp(-(x-x_0)/\tau_1) + A_2*\exp(-(x-x_0)/\tau_2)$.

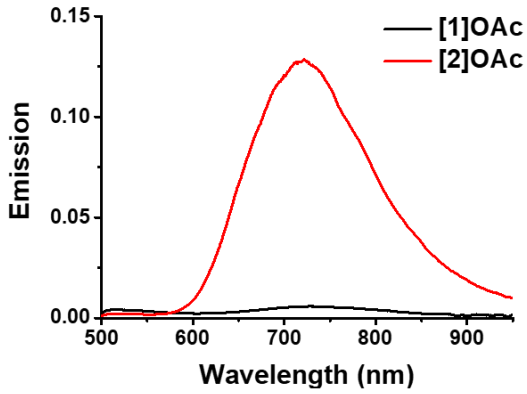

Figure AIII.5 The solid emission spectra of complexes **[1]OAc** and **[2]OAc** (excitation 450 nm, laser intensity 50 mW cm^{-2}, Edmund optics high-pass filter was used to filter the spectra below 500 nm).

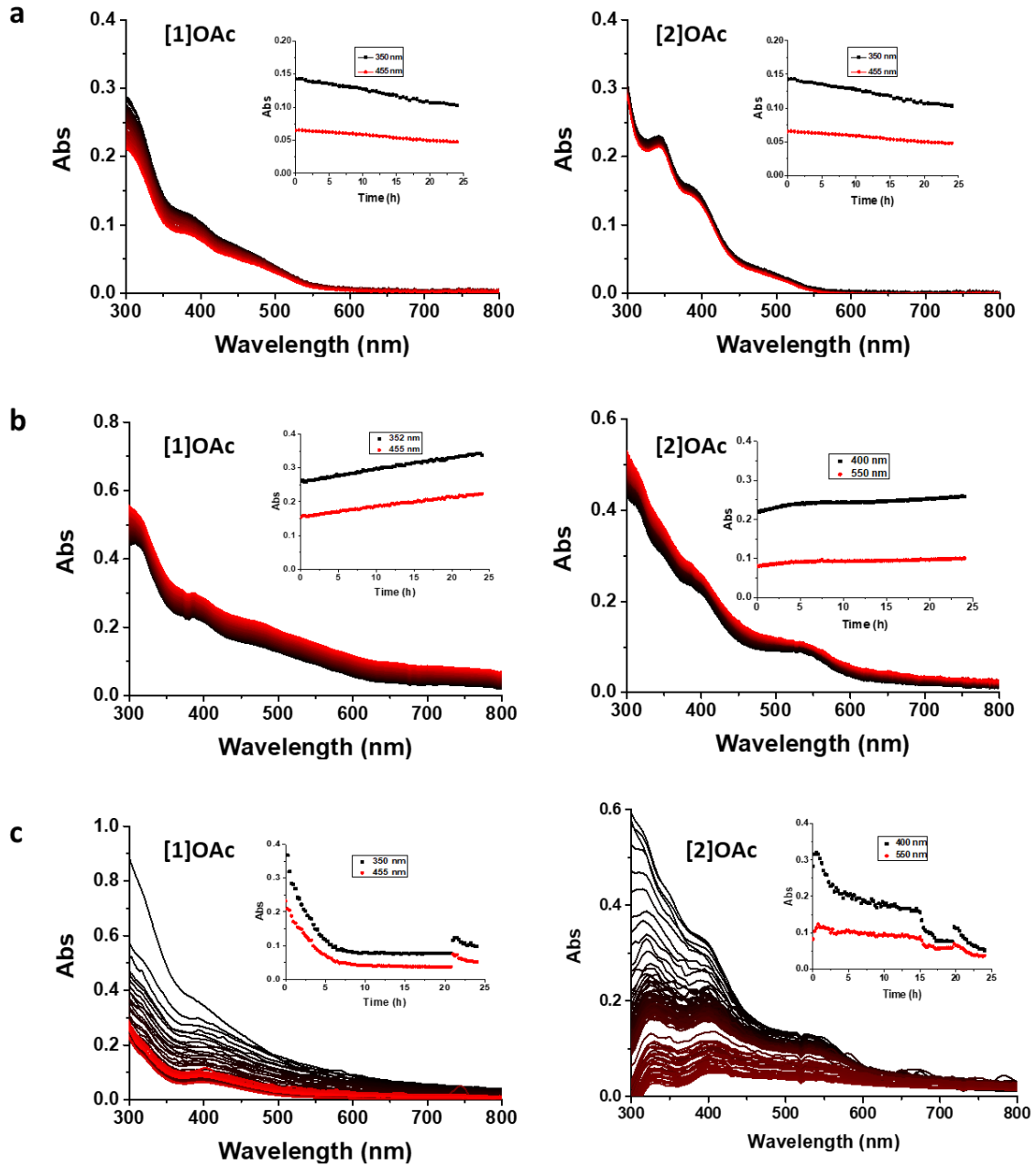

Figure AIII.6 Time evolution for 24 h of the absorbance spectra of solutions of **[1]OAc** and **[2]OAc** (50 µM) in PBS (a), OptiMEM with (b) or without (c) FCS medium (2.5 % v/v). Interval: 15 min, from black (0 h) to red (24 h).

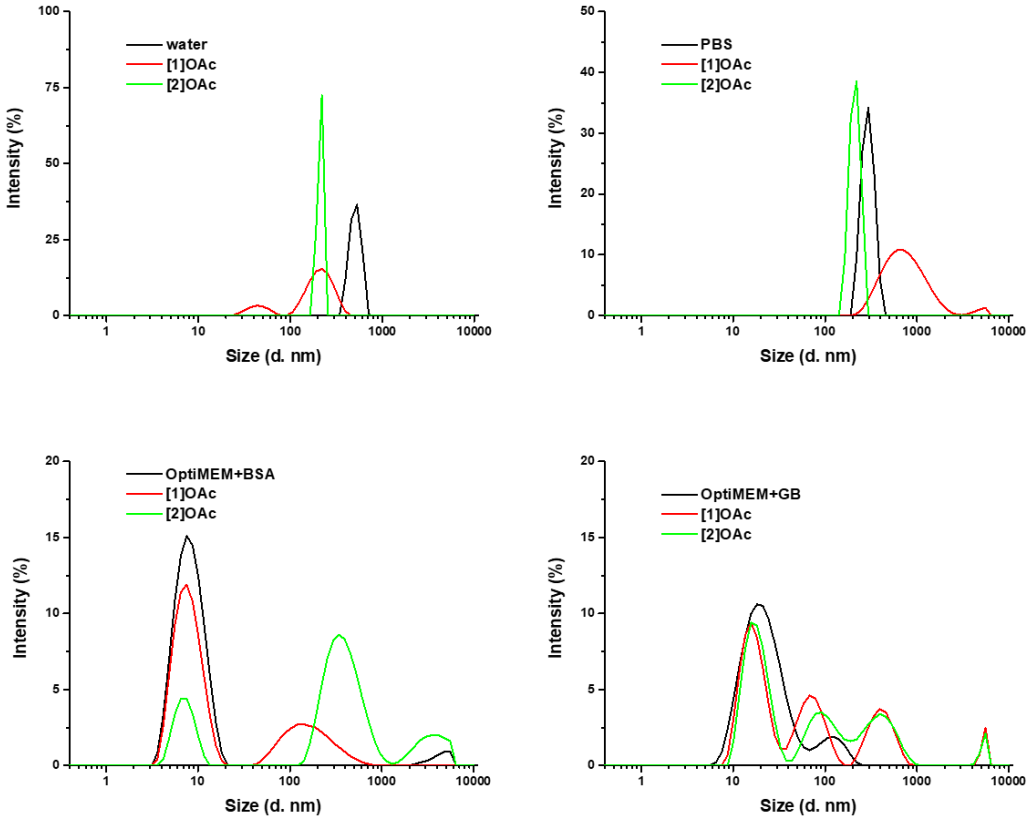

Figure AIII.7 Size distribution observed by Dynamic Light Scattering (DLS) for **[1]OAc** and **[2]OAc** (50 µM) dissolved in different buffers. PBS = phosphate buffer saline; BSA = bovine serum albumin (50 g/L in Opti-MEM medium); GB = globulin (30 g/L in Opti-MEM medium).

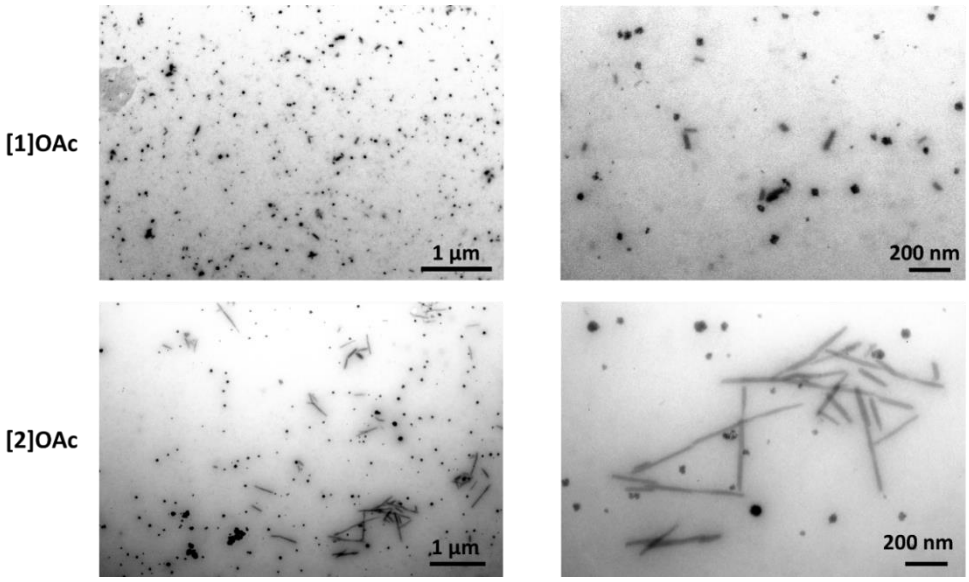

Figure AIII.8 TEM images of **[1]OAc** and **[2]OAc** (50 µM) in Opti-MEM with FCS (2.5 % v/v).

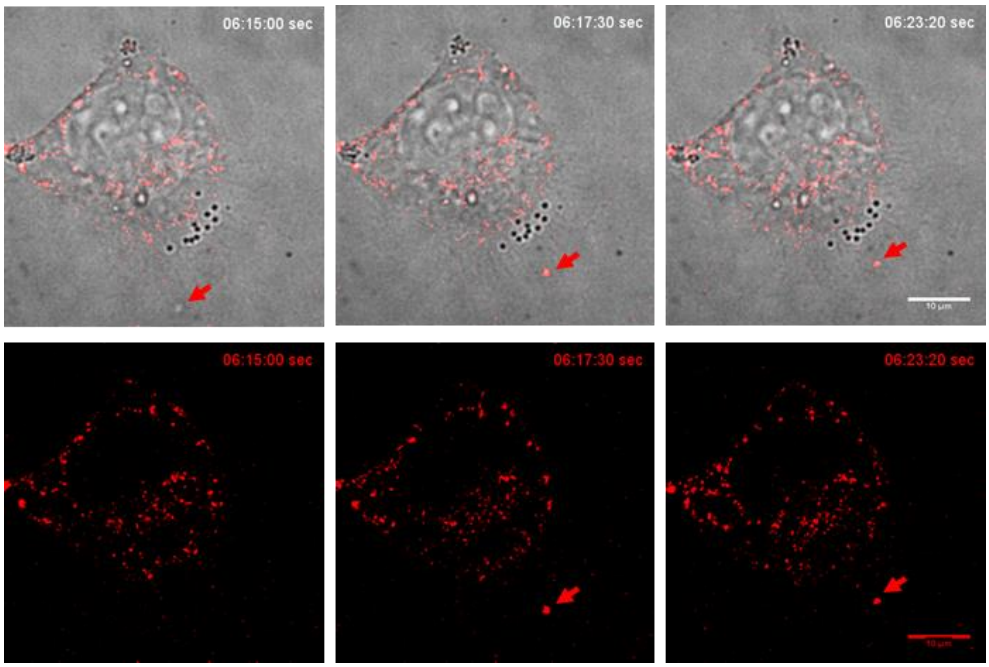

Figure AIII.9 Selected timepoints from 16-h time-lapse confocal fluorescence live-cell imaging of **[1]OAc** uptake by A549 cells. The complex was added in the dish 15 min before initiation of the measurement (t=0). The top row shows overlayed bright field and **[1]OAc** fluorescence images. The bottom row shows **[1]OAc** fluorescence images. Red arrows indicate **[1]OAc** uptake by the cell. Brightfield and fluorescence (561 nm excitation) images were acquired every 50 s. Time is indicated in hours:minutes:seconds format. The selected time points are extracted from Video S1.

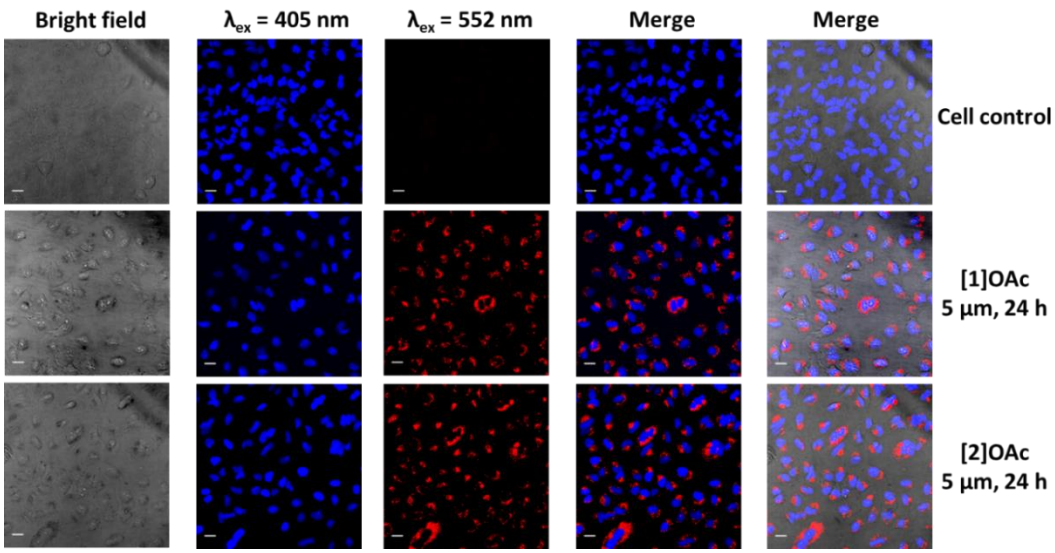

Figure AIII.10 Confocal images of A549 cells treated with or without complexes **[1]OAc** and **[2]OAc** (red, 650-750 nm, λ_{ex} = 552 nm), and staining with Hoechst 33342 (blue, 420-480 nm, λ_{ex} = 405 nm). Scale bar: 20 µm. complex concentration 5 µM, Pearson coefficients -1.

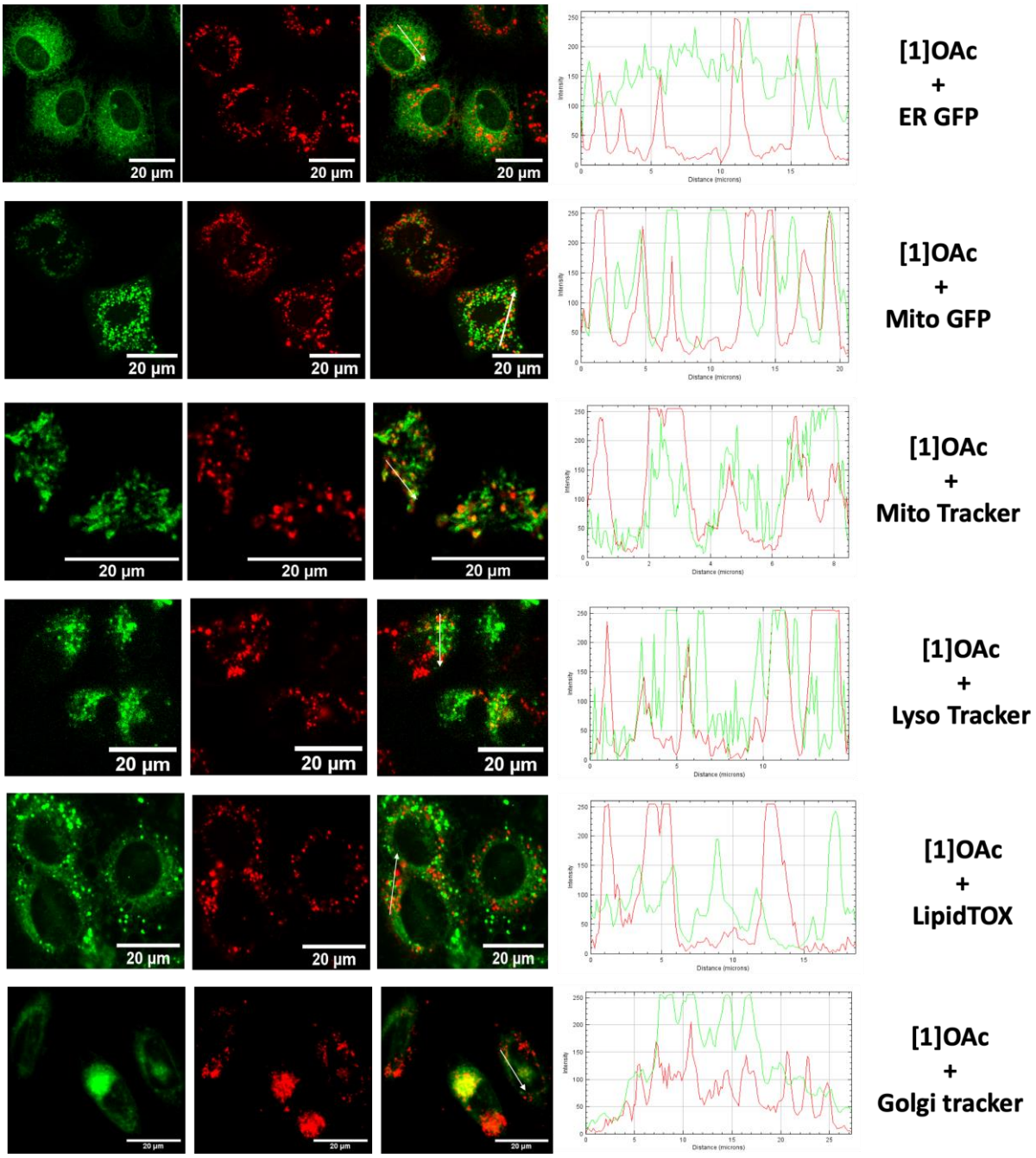

Figure AIII.11 Confocal microscopy overlapping images and pixel intensity curves for A549 cells co-treated with complexes **[1]OAc** (red, 5 µM) and (green) dyes Endoplasmic reticulum Green Fluorescent Protein (GFP), Mitochondria GFP, MitoTracker Green FM, LysoTracker™ Green DND-26, HCS LipidTOX™ Green Neutral Lipid Stain and BODIPY™ FL C5-Ceramide complexed to BSA Golgi. Green channel (λ_{ex} = 488 nm, λ_{em} = 500-530 nm). Red channel (λ_{ex} = 552 nm, λ_{em} = 650-750 nm).

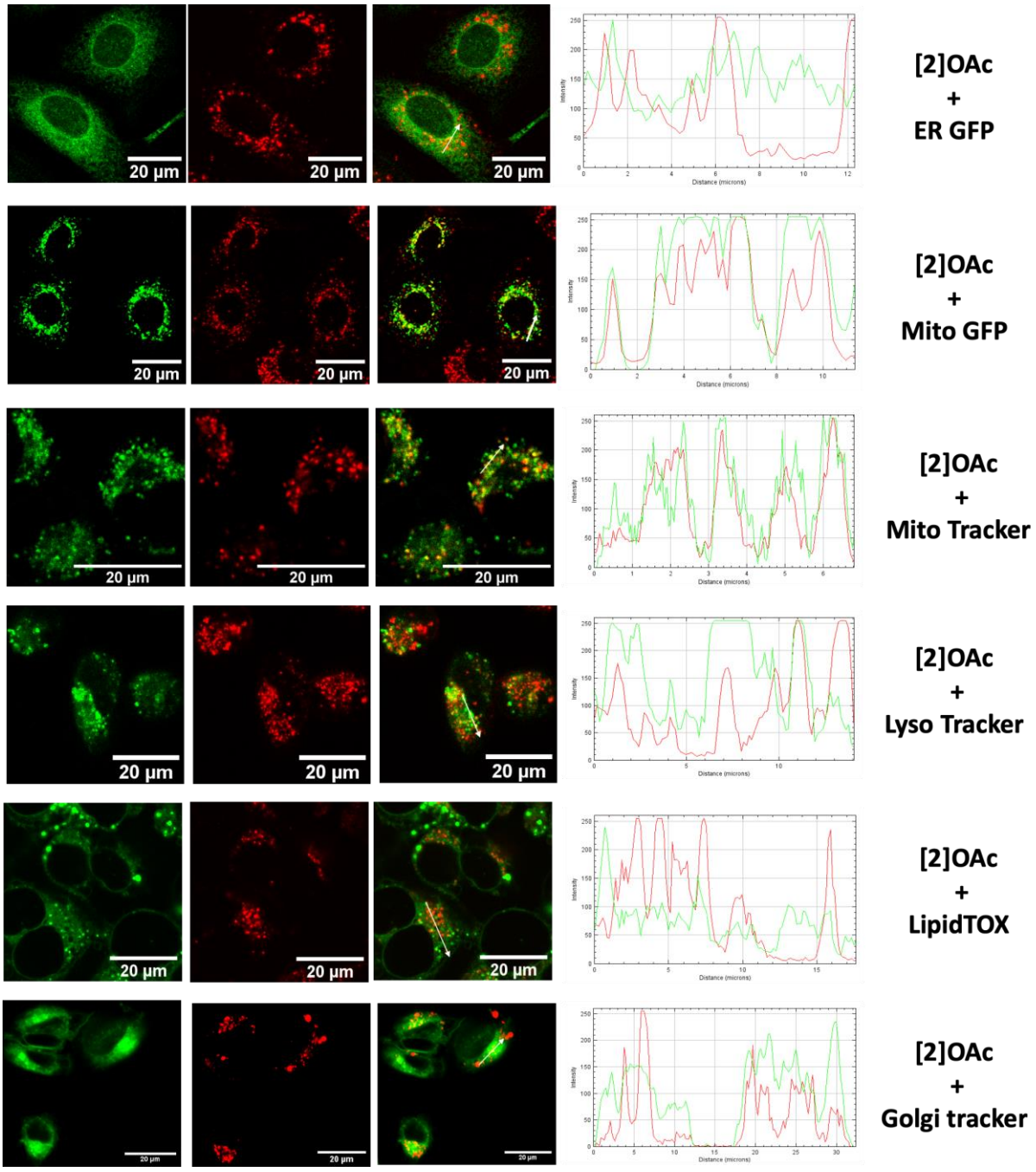

Figure AIII.12 Confocal microscopy overlapping images and pixel intensity curves for A549 cells co-treated with complex **[2]OAc** (red, 5 µM) and (green) dyes Endoplasmic reticulum Green Fluorescent Protein (GFP), Mitochondria GFP, MitoTracker Green FM, LysoTracker™ Green DND-26, HCS LipidTOX™ Green Neutral Lipid Stain and BODIPY™ FL C5-Ceramide complexed to BSA Golgi. Green channel (λ_{ex} = 488 nm, λ_{em} = 500 – 530 nm). Red channel (λ_{ex} = 552 nm, λ_{em} = 650 – 750 nm).

Table AIII.2 Pearson's correlation coefficients measured for co-localization studies of complexes **[1]OAc** or **[2]OAc** and different organelle-staining dyes in confocal cell imaging shown in Figure S15 and S16.

Dye	**Complex**	
	[1]OAc	**[2]OAc**
Endoplasmic reticulum GFP	-0.1 to 0.2	-0.1 to 0.2
Mitochondria GFP	-0.2 to 0.4	0.3 to 0.6
MitoTracker Green FM	0.2 to 0.4	0.3 to 0.5
LysoTracker™ Green DND-26	-0.3 to 0.1	0.0 to 0.3
HCS LipidTOX™ Green Neutral Lipid Stain	0.0 to 0.1	-0.1 to 0.1
BODIPY™ FL C5-Ceramide complexed to BSA golgi Dye	0.5 to 0.7	-0.4 to 0.6

Table AIII.3 Platinum cellular uptake according to ICP-MS analysis in A549 cells treated with **[1]OAc** and **[2]OAc** (5 µM, 1 mL) in combination with different inhibition conditions after 2 h.

Complex	**inhibitor**	**uptake (ng Pd/million cells)**	**Inhibition percent** [a]
[1]OAc	control	111±25	0%
	dynasore	84±7	24%
	4 °C	52±2	53%
[2]OAc	control	159±5	0%
	dynasore	58±7	64%
	4 °C	66±8	58%

[a] Inhibition percent = $(\text{uptake}_{\text{control}}-\text{uptake}_{\text{inhibitor}})/\text{uptake}_{\text{control}} \times 100\%$.

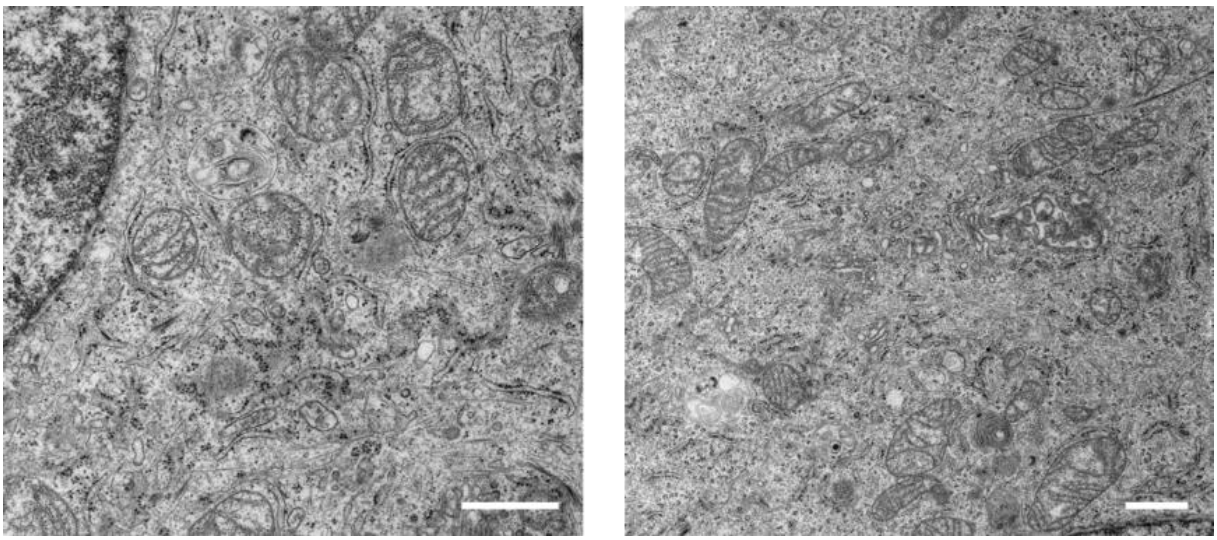

Figure AIII.13 Electron Microscopy imaging of control A549 cells without platinum treatment (scale bar 1 µM).

APPENDIX IV SUPPORTING INFORMATION FOR CHAPTER 5

Table AIV.1 Selected bond distances (Å) and angels (degree) in the crystal structure of **PdL**.

Distance (Å)		Angel (˚)	
Pd-N1	2.144(3)	C11-Pd1-C17	92.09(12)
Pd-C11	1.969(3)	C11-Pd1-N1	80.17(11)
Pd-C17	1.972(3)	C17-Pd1-N1	171.99(11)
Pd-N3	2.163(3)	C17-Pd1-N3	80.24(11)˚
Pd-Pd	3.518	N1-Pd1-N3	107.42(10)

Table AIV.2 TDDFT singlet-singlet transitions calculation information of **PdL** in monomeric or dimeric state.

State	**Energy (nm)**	**Energy (eV)**	**Oscillator strength (f)**	**Orbital transition contribution**
Monomer	383.0	4.0697	0.1262	HOMO→LUMO 89.9%
	335.2	3.6989	0.3642	HOMO→LUMO+1 84.7%
	304.65	3.2369	0.7603	HOMO-1→LUMO 70.9%
Dimer	540.1232	2.2955	0.0043	HOMO→LUMO 100%
	501.6673	2.4714	0.0484	HOMO→LUMO 96%
	450.6614	2.7512	0.0168	HOMO→LUMO 47.3% HOMO-1→LUMO 36.9%
	400.7565	3.0938	0.0819	HOMO→LUMO+1 86.4%

Table AIV.3 The photophysical properties of **PdL** in monomeric state.

Solvent	**λ_{abs}, nm (ε x 10^3 M^{-1} cm^{-1})[a]**	**λ_{em} (nm)[a,b]**	**lifetime (ns)[a,d]**	**φ_P [c]**	**φ_Δ [c]**
DMSO	343 (25.8), 405 (5.2), 481 (3.7)	564	0.406 ± 0.004	0.0008	0.09
THF	347 (22.5), 410 (4.3), 480 (2.9)	540	0.432±0.005		

[a] measurement were carried out in aerated DMSO or THF
[b] excitation and concentration: 419 nm, 100 µM.
[c] measurement was carried out in MeOD.
[d] excitation source : 340 nm. Monoexponential model: $y = y_0 + A_1 * \exp[-(x-x_0)\tau_1]$

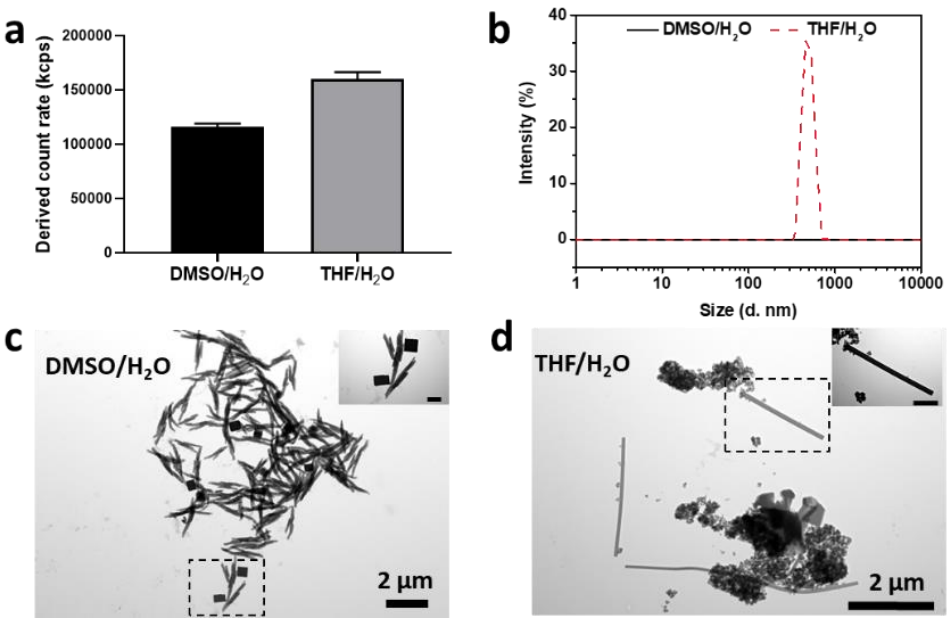

Figure AIV.1 (a) DLS derived count rate in the DMSO/H_2O or THF/H_2O system of **PdL** (100 µM) after 30 min self-assembly; (b) Size distribution of the DLS analysis in the DMSO/H_2O or THF/H_2O system of **PdL** (100 µM) after 30 min self-assembly; TEM images of samples prepared from the DMSO/H_2O (c) or THF/H_2O (d) system of **PdL** (100 µM) after 30 min self-assembly. Inset picture scale bar: 500 nm.

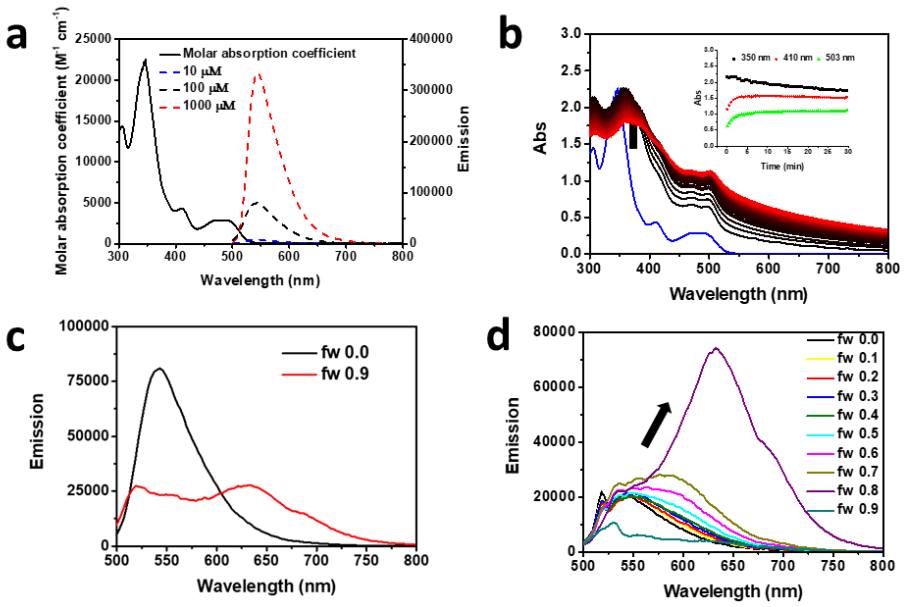

Figure AIV.2 (a) The molar absorption coefficient (black solid line) and emission spectra of **PdL** in tetrahydrofuran (THF) solution at different concentrations (blue dash line 10 µM; black dash line 100 µM, red dash line 1000 µM). (b) Time evolution of the absorption spectra of H_2O/THF solution (100 µM, 9:1, v/v) of **PdL** at 298 K for 30 min (30 s interval, the color of

spectra change from black (0 min) to red (30 min); the blue line is the absorbance spectra of **PdL** (100 µM) in pure THF). Inset: time evolution of the absorption at 350 nm (black square), 480 nm (red dot), 504 nm (green triangle) of the solution. (d) Emission spectra of **PdL** (100 µM) in pure THF (fw (V_{water}/V_{total}) = 0.0) and water/THF mixture (9:1, v/v, fw = 0.9); excitation 419 nm. (d) Emission spectra of **PdL** (20 µM) in different THF/water ratio (from v/v = 10/0 to 1/9, excitation 450 nm).

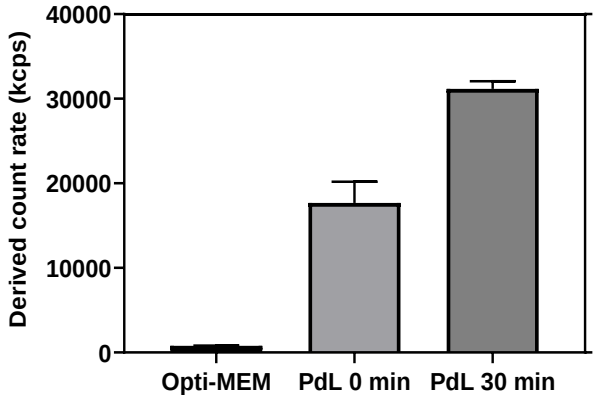

Figure AIV.3 DLS scattering-derived count rate of **PdL** in Opti-MEM complete medium at 0 and 30 min under room temperature.

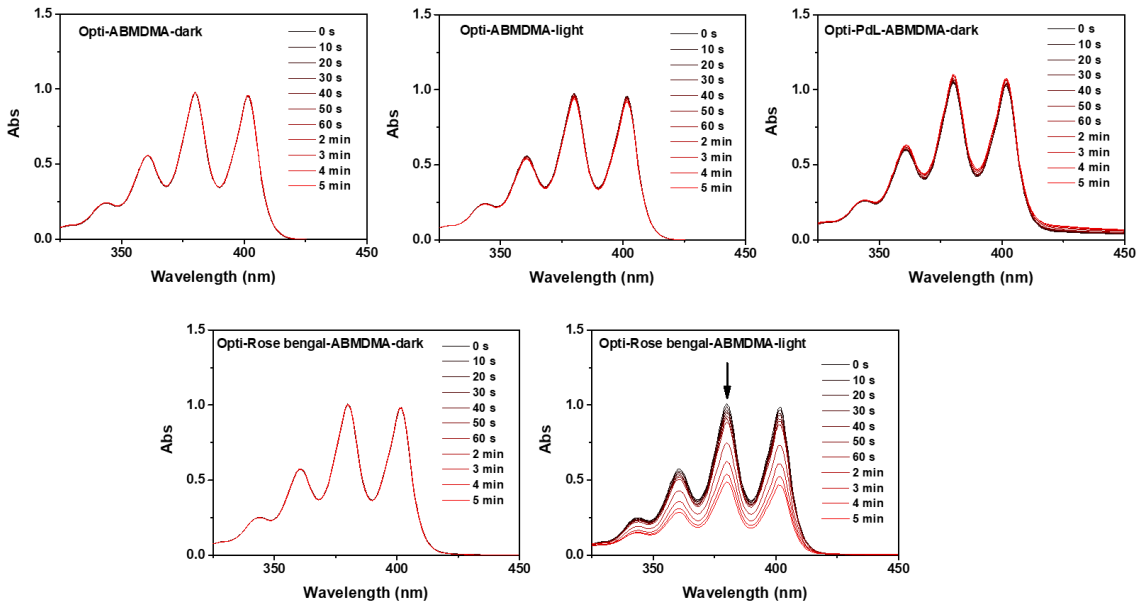

Figure AIV.4 Time evolution of the absorption spectrum of an Opti-MEM complete solution of 9,10-anthracenediyl-bis(methylene)-dimalonic acid (ABMDMA, 100 µM) in the absence or presence of **PdL** (25 µM) or rose Bengal, under green light irradiation (515 nm).

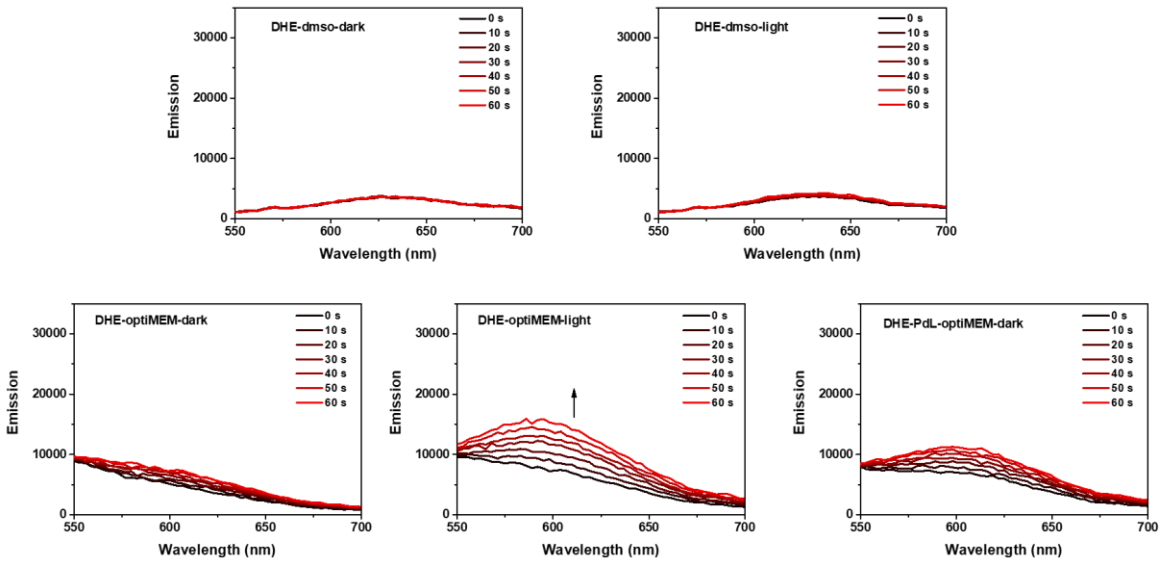

Figure AIV.5 The emission spectra of dihydroethidium (DHE) solution (DMSO or Opti-MEM complete) in the absence or presence of **PdL** (25 µM) under green light irradiation (520 nm) or in the dark, over 60 s.

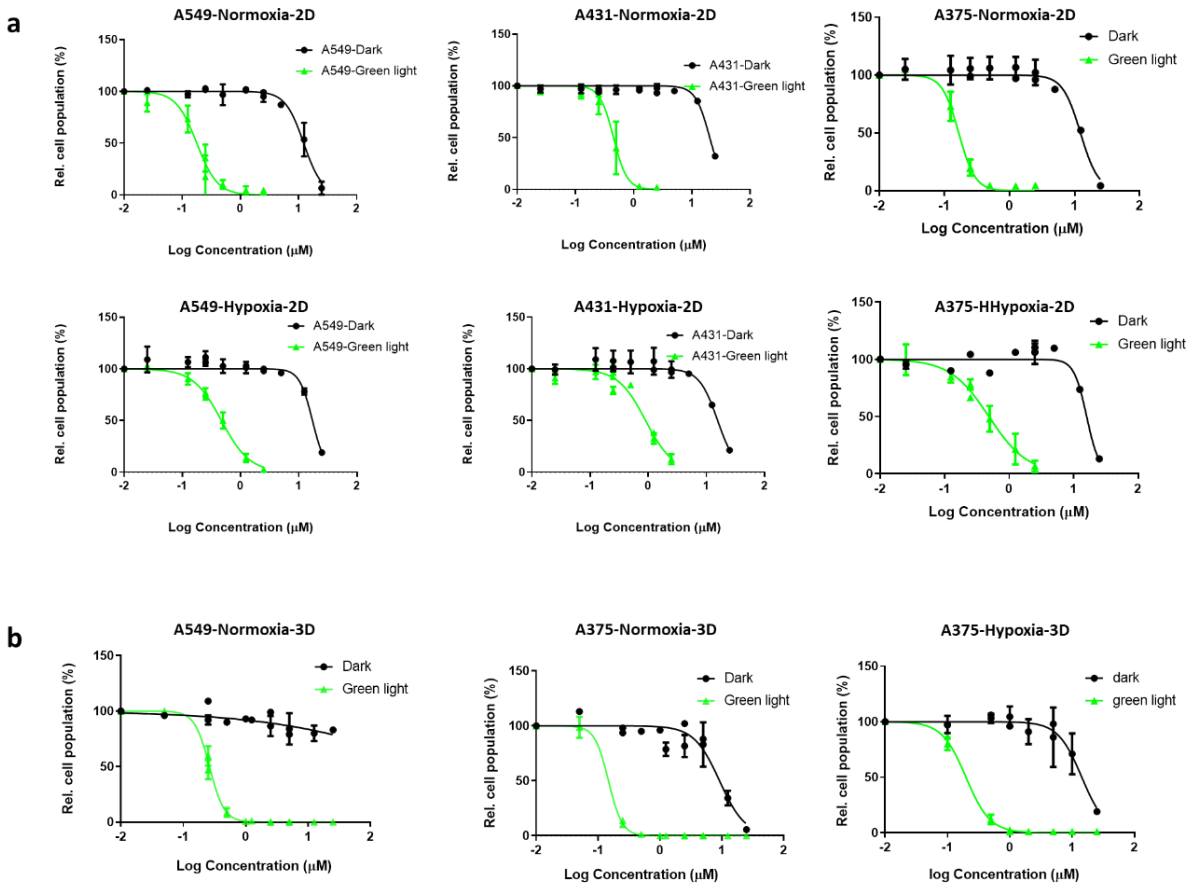

Figure AIV.6 Dose-response curves for 2D-monolayer (a) or 3D-spheroid (b) for different human cancer cell lines incubated with **PdL**, either in the dark (black data points) or upon green

light irradiation (green data points) under normoxic-2D (520 nm, 20 min, 10.92 mW/cm^2, 13 J/cm^2), hypoxic-2D (520 nm, 32 min, 6.90 mW/cm^2, 13 J/cm^2), normoxia-3D spheroid condition (520 nm, 32 min, 6.90 mW/cm^2, 13 J/cm^2), or hypoxia-3D spheroid condition (520 nm, 55 min, 3.99 mW/cm^2, 13 J/cm^2).

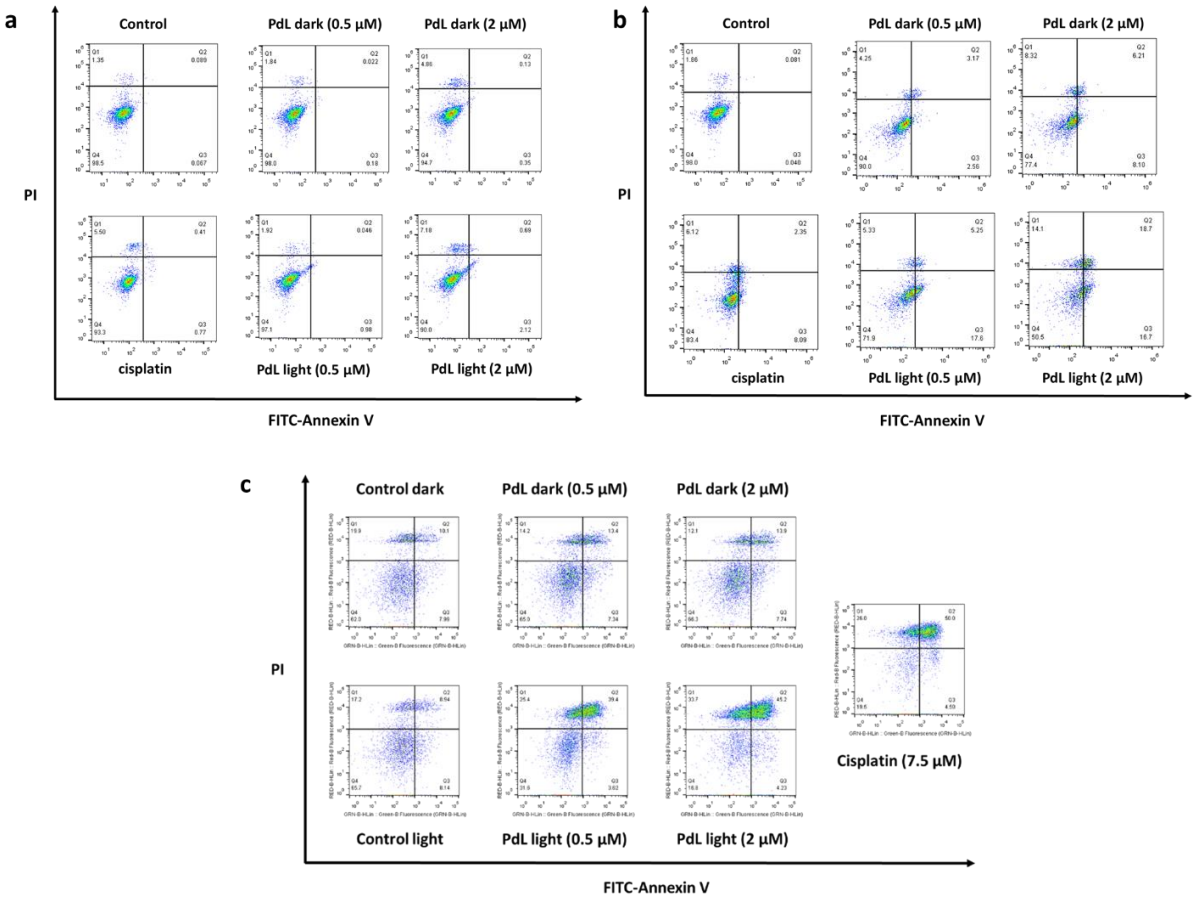

Figure AIV.7 Annexin V/Propidium iodide double staining FACS data for A375 cells after treatment with cisplatin (7.5 µM) or **PdL** (0.5 µM or 2 µM) in the dark or upon green light irradiation (normoxic 520 nm, 20 min, 10.9 mW/cm^2, 13 J/cm^2) after 2 (a), 4 (b) and 24 h (c)

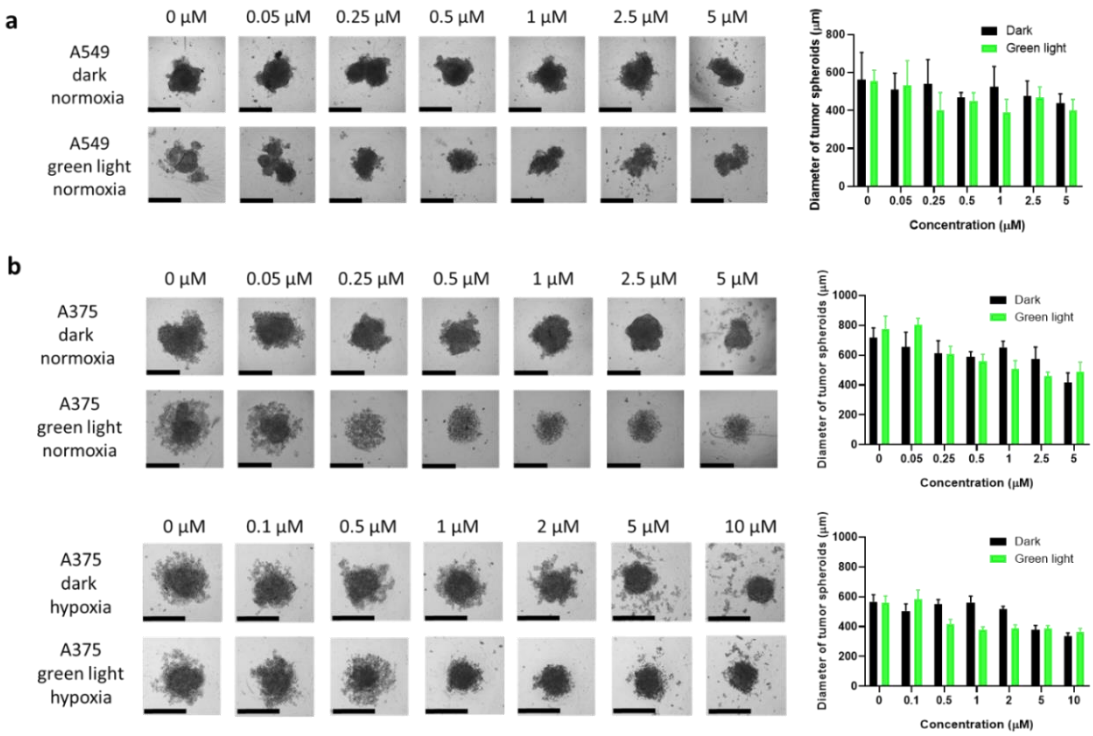

Figure AIV.8 Bright filed images (left) and diameter (right, µm) for A549 (a) and A375 (b) 3D tumor spheroids kept in the dark (black bars) or irradiated with green light (green bars, 520 nm, 13 J/cm^2). Scar bar 500 µm.

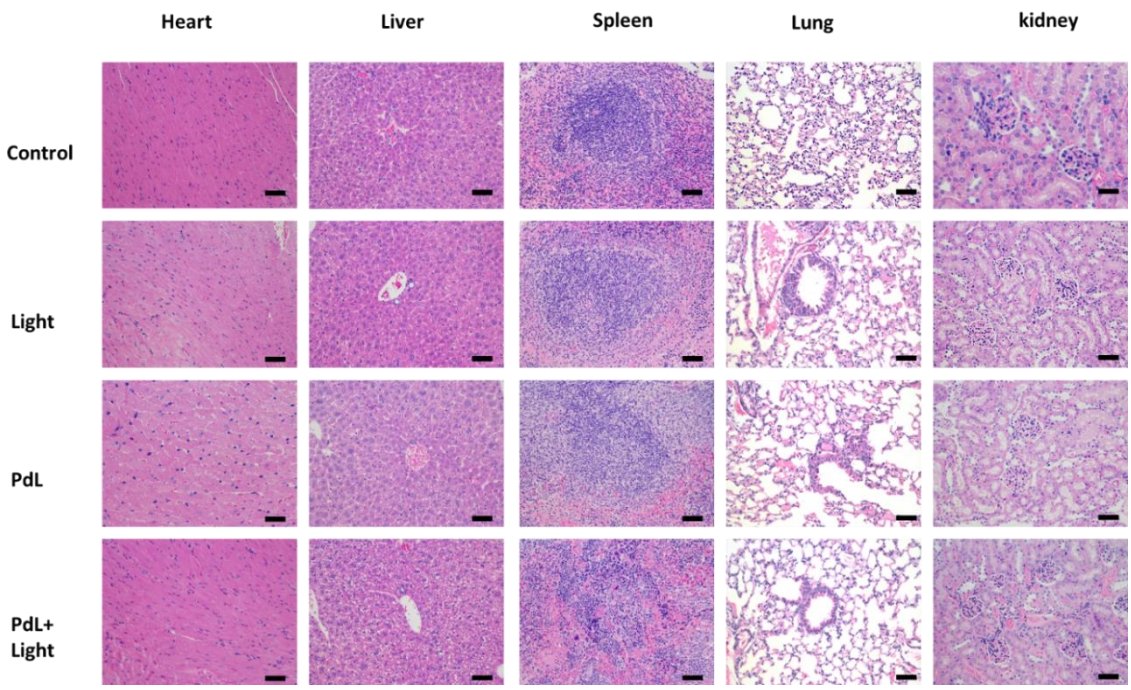

Figure AIV.9 The H&E staining of different mice organs after treatment with vehicle control or **PdL**, and either without or with green light irradiation (100 mW/cm^2, 10 min, 60 J/cm^2). Scale bar 200 µm.

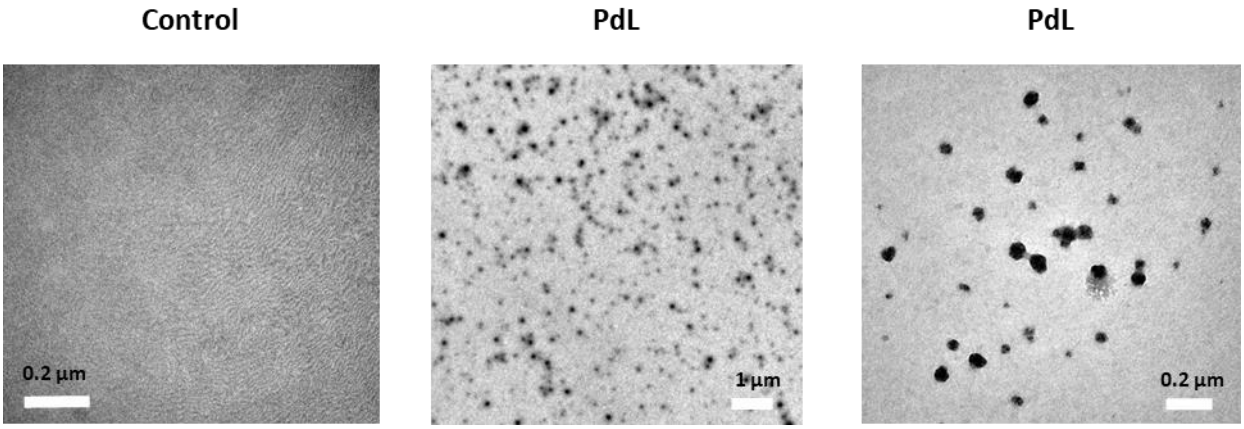

Figure AIV.10 EM images showing the morphology of nanoparticles found in the blood of mice 12 h after intravenous tail injection of **PdL** (middle and right images), or in an untreated control mice (left image). Injection dose: 2.1 µmol/kg, 0.9 mg/kg, 420 µM, 100 µL saline.

APPENDIX V SUPPORTING INFORMATION FOR CHAPTER 6

Table AV1. The selected bond distances (Å) and angels (°) of **[1]Cl** and **[2]AuCl$_4$**.

[1]Cl		**[2]AuCl$_4$**	
Au-C28	2.030(7)	Au-N3	1.995(18)
Au-N3	2.046(6)	Au-N6	2.00(2)
Au-N4	2.050(6)	Au-N4	2.002(16)
Au-C1	2.060(5)	Au-N1	2.081(18)
C28-Au-N3	166.6(6)	N3-Au-N6	167.2(13)
C28-Au-N4	92.7(3)	N3-Au-N4	81.4(6)
N3A Au-N4A	81.5(3)	N6-Au-N4	93.2(9)
C28-Au-C1	96.5(3)	N3-Au-N1	88.8(9)
N3-Au-C1	91.3(3)	N6-Au-N1	99.0(7)
N4-Au-C1	166.9(4)	N4-Au-N1	163.0(13)

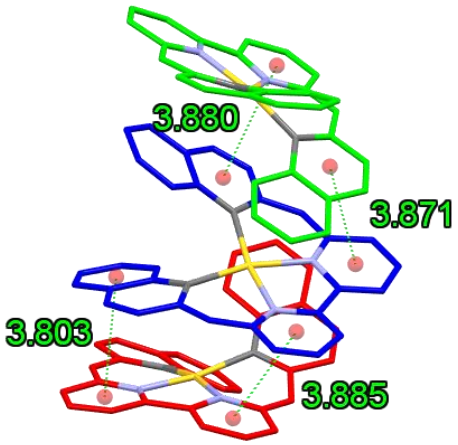

Figure AV1. The crystal packing structure of **[1]Cl** with the intermolecular π-π stacking distance. The H and counterions were omitted for clarity.

Table AV2. The TDDFT singlet-singlet transitions calculation information of gold complexes.

Complex	**Energy (nm)**	**Energy (eV)**	**Oscillator strength (f)**	**Orbital transition contribution**
[1]$^+$	451	2.7451	0.2282	97.4% HOMO→LUMO
	370	3.3471	0.1146	95.6% HOMO-1→LUMO
	694	1.7863	0.0074	97.8% HOMO→LUMO
[2]$^+$	531	2.3334	0.0066	98.1% HOMO-1→LUMO
	469	2.6413	0.1915	95.9% HOMO→LUMO+1

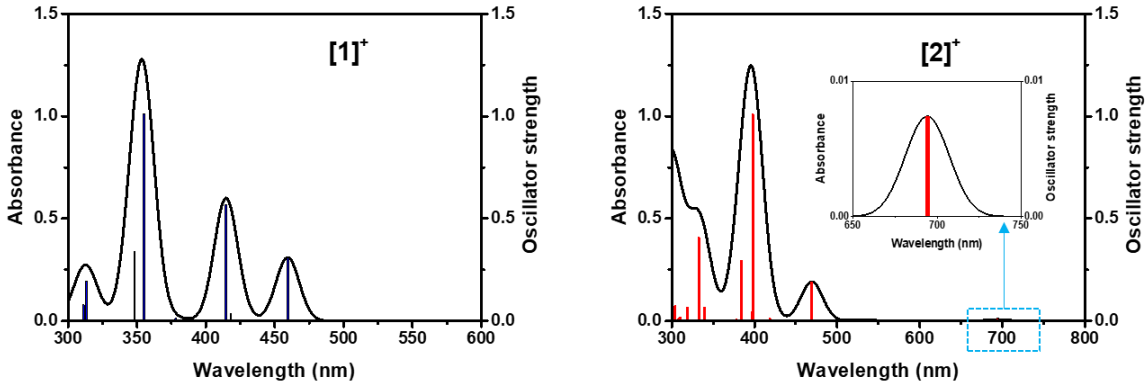

Figure AV2. The TDDFT absorbance peaks and spectra of **[1]**$^{+}$ and **[2]**$^{+}$.

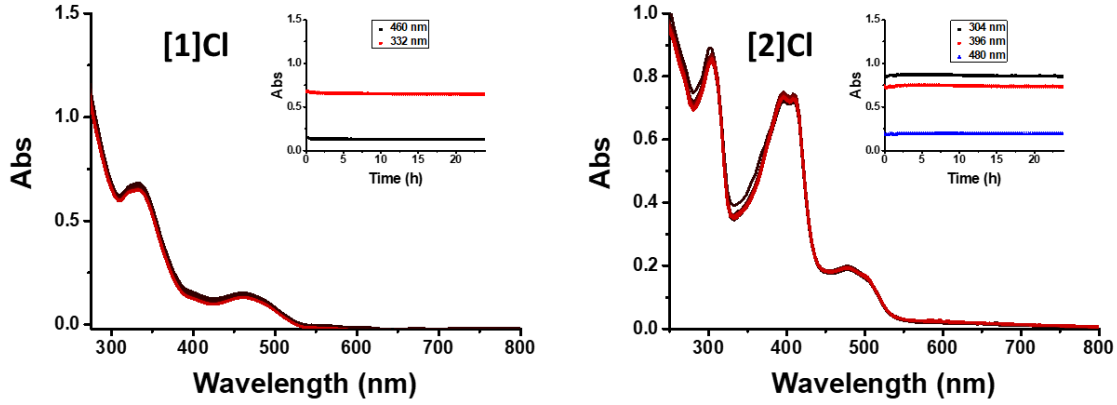

Figure AV3. Time evolution of the absorbance spectrum of **[1]Cl** and **[2]Cl** (50 µM) in PBS solution (100 µM) for 24 hours at 37 °C; measurement interval 15 min, color changes from black (0 s) to red (24 h).

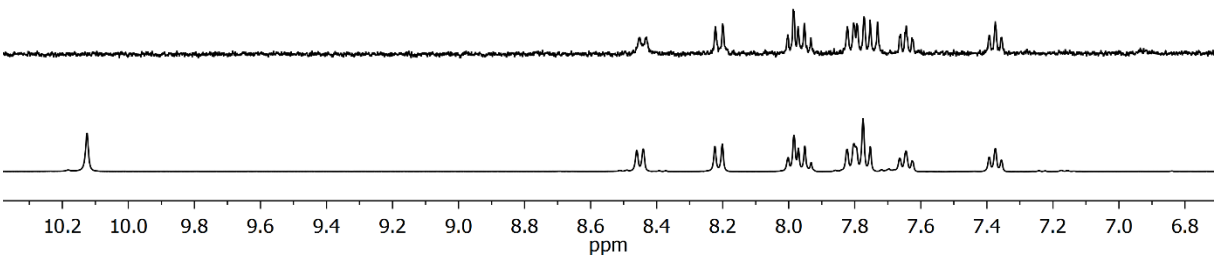

Figure AV4. ^{1}H NMR of the precipitate formed after 24 h of incubation of compound **[2]Cl** (3.0 mM) and GSH (6.0 mM) at a ratio of 1:2 (top) and spectra of H_2biqbpy2 (bottom) added as a reference for peak identification. All spectra were measured in DMSO-d_6 at 25 ºC.

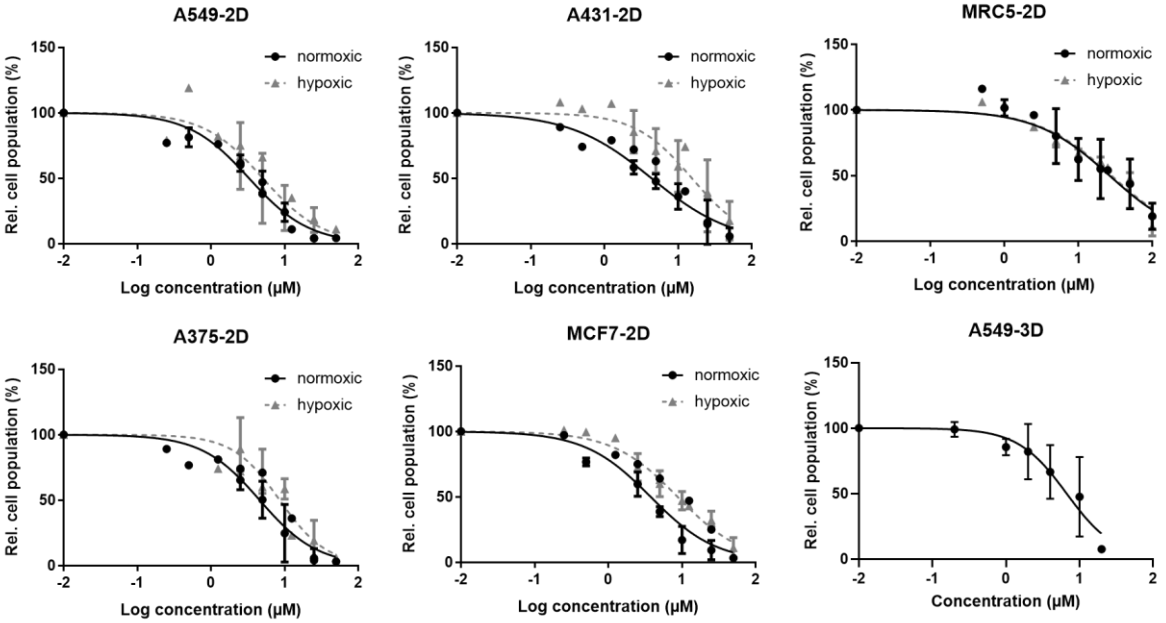

Figure AV5. Dose-response curves for four cancer cells and one healthy skin cells incubated with **[1]Cl** under normoxic or hypoxic conditions, in the 2D-monolayer or 3D-spheroid model.

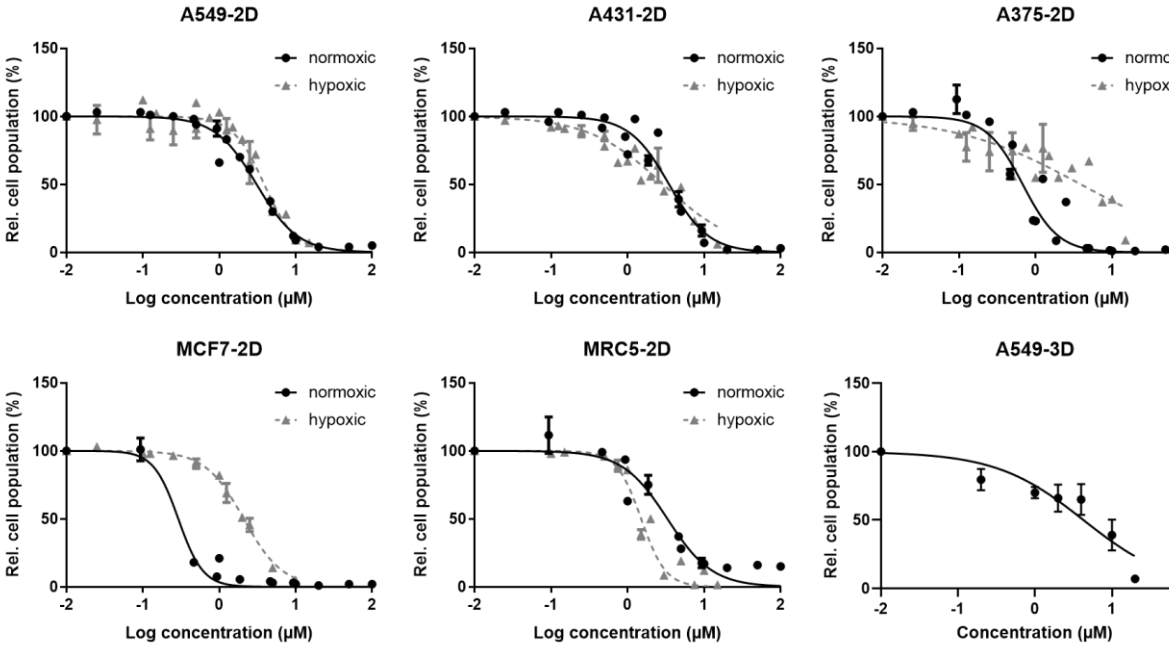

Figure AV6. Dose-response curves for four cancer cells and one healthy skin cells incubated with **[2]Cl** under normoxic or hypoxic conditions, in the 2D-monolayer or 3D-spheroid model.

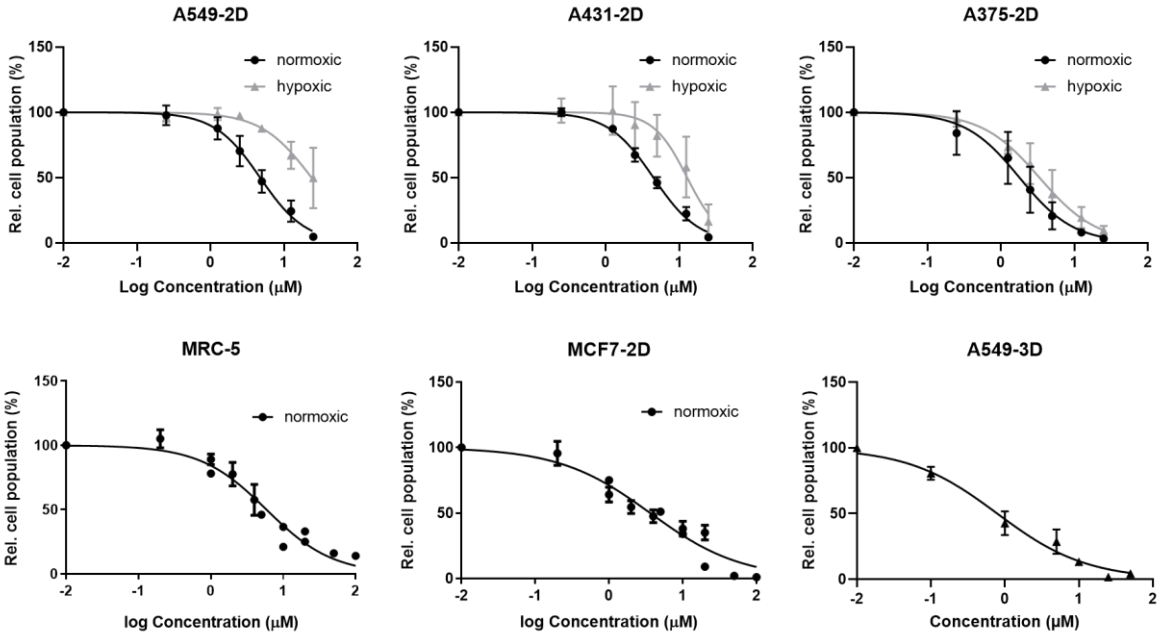

Figure AV7. Dose-response curves for four cancer cells and one healthy skin cells incubated with cisplatin under normoxic or hypoxic conditions, in the 2D-monolayer or 3D-spheroid model.

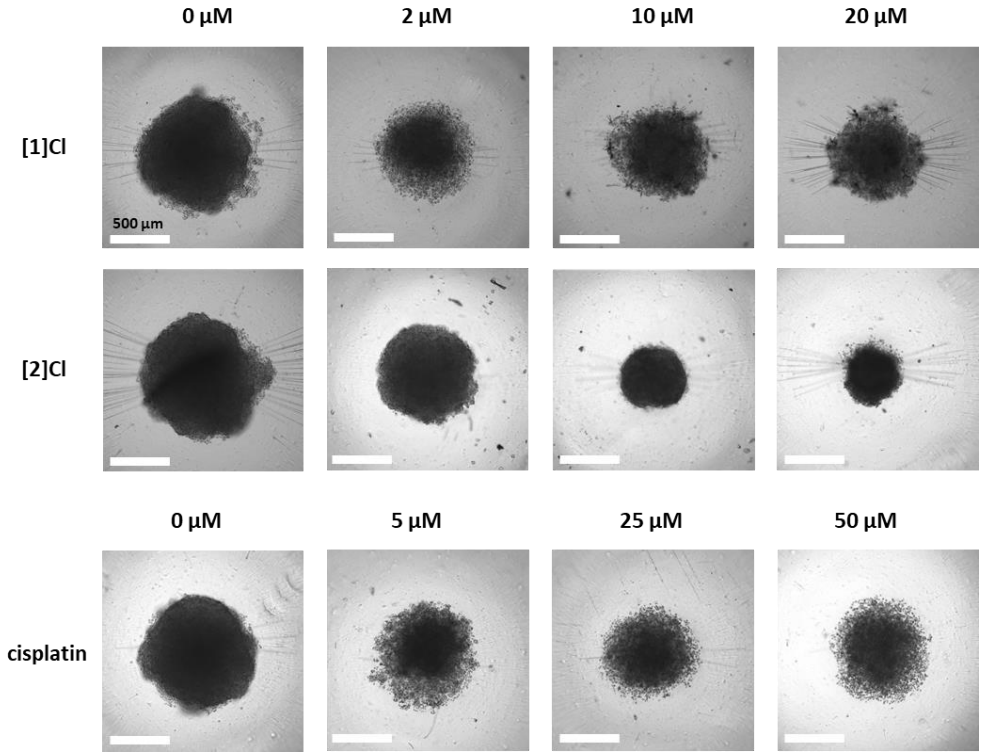

Figure AV8. Bright-field imaging of 3D tumor spheroids treated with gold complexes or vehicle control (DMSO); scale bar is 500 µm. The cells were seeded at t=0 (500 cells per well), treated at t=4 days, measured (diameter) at t=7 days.